2012

Applications of manganese-enhanced magnetic resonance imaging in neuroscience

McCreary, J. Keiko

Lethbridge, Alta. : University of Lethbridge, Dept. of Neuroscience, c2012

APPLICATIONS OF MANGANESE-ENHANCED MAGNETIC RESONANCE IMAGING IN NEUROSCIENCE

J. KEIKO McCREARY
BA.Sc., University of Lethbridge, 2010

A Thesis
Submitted to the School of Graduate Studies
Of the University of Lethbridge
In Partial Fulfillment of the
Requirements for the Degree

MASTER OF SCIENCE

Department of Neuroscience
University of Lethbridge
LETHBRIDGE, ALBERTA, CANADA

I dedicate this thesis in memory of Aunty Naomi, Uncle Jim, Grandma Betty and Grandpa Allen.

APPLICATIONS OF MANGANESE-ENHANCED MAGNETIC RESONANCE IMAGING IN NEUROSCIENCE

ABSTRACT

Manganese-Enhanced Magnetic Resonance Imaging (MEMRI) has proven itself to be a beneficial technique in the field of Neuroscience. This thesis applies MEMRI to studies in neuroscience by first establishing the limitations concerning the use of MEMRI in live rats. Experiment 1 used an osmotic pump for manganese (Mn) delivery to the lateral ventricles for acquisition of anatomical images using MEMRI. From my knowledge, this was the first method demonstrating slow infusion of Mn to the lateral ventricles. In Experiment 2, MEMRI was used for volumetric analysis the whole brain and hippocampus of prenatally stressed rats. To my knowledge, this study was the first to investigate the effect of generational prenatal stress on the structure of a rat's brain using MEMRI and histology. Additionally, Experiment 2 investigated the use of a subcutaneous osmotic pump to deliver Mn for MEMRI. A summary on the use of MEMRI in Neuroscience concludes this thesis, with a discussion on the methods used and related technical considerations.

ACKNOWLEDGEMENTS

This thesis would not have been possible without the guidance, support and help of many individuals who in one way or another helped me to complete this task of obtaining my MSc in Neuroscience.

First, I would like to thank my supervisors Dr. Albert Cross and Dr. Gerlinde Metz. Dr. Cross, thank you for teaching me about MRI and its applications; and for showing me that physics is really not that bad. Dr. Metz, thank you for allowing me to complete my undergraduate independent study in your lab and for kick starting my passion for Neuroscience. Your kindness, compassion and encouragement will forever be remembered.

To my committee members; Dr. Matt Tata, Dr. Craig Coburn and Dr. Andrew Iwaniuk; thank you for your advice, guidance, and support. To the Cross and Metz labs; your helpfulness, patience and friendship has been invaluable both academically and personally; for this I am truly grateful.

To my friends who put up with my busy schedule and absence throughout the last two years, thank you for your patience and loyalty. To Patrick, thank you for your support, patience, help and love. I am forever and always grateful.

Lastly, to my family; thank you for your unwavering support. Mom, Dad and Kris, thank you for teaching me that hard work and kindness does pay off. Love you more.

TABLE OF CONTENTS

LIST OF TABLES

LIST OF FIGURES

LIST OF ABBREVIATIONS

B0	External magnetic Field
B1	Transverse Oscillating Field
BBB	Blood-Brain-Barrier
BCB	Blood-CSF-Barrier
CA1	Cornu ammonis 1
CA2	Cornu ammonis 2
CA3	Cornu ammonis 3
Ca^{2+}	Calcium Ion
CSF	Cerebrospinal Fluid
EC	Entorhinal Cortex
F0	Parental Generation
F1	Offspring
F2	Grand Offspring
F3	Great Grand Offspring
HPA	Hypothalamic-pituitary-Adrenal axis
IP	Intraperitoneal
MEMRI	Manganese-Enhanced Magnetic Resonance Imaging
Mg^{2+}	Magnesium
Mn	Manganese
$MnCl_2$	Manganese Chloride
MRI	Magnetic Resonance Imaging
MSDS	Material Safety Data Sheet
Na^{2+}	Sodium Ion
NMR	Nuclear Magnetic Resonance
P	Postnatal Day
PBS	Phosphate Buffer Solution
PFA	Paraformaldehyde
PS	Prenatal stress
RF	Radio Frequency
ROI	Region of Interest
SD	Standard deviation
SE	Spin-Echo
SEM	Standard Error of the Mean
SNR	Signal to Noise Ratio
SQ	Subcutaneous
T1	Longitudinal Relaxation
T2	Transverse Relaxation
TE	Echo Time
TPS	Transgenerational Prenatal Stress
TR	Repetition Time

CHAPTER 1

Introduction

1.1 Introduction to Magnetic Resonance Imaging

Anatomical and functional mapping of the brain has been a fundamental goal of modern neuroscience since the early 1900's. In the past three decades, the magnetic resonance imaging technique has emerged as the single most powerful neuroimaging tool to accomplish this goal. Advances in magnetic resonance imaging give exceptional information on the anatomy, physiology and functional processes of the brain. The search for methods of obtaining more detailed physiological, molecular and functional information from magnetic resonance imaging (MRI) is becoming more prominent and the interest in the use of new contrast agents is increasing.

MRI uses the principles of nuclear magnetic resonance (NMR) which was first observed in bulk matter by Felix Bloch and Edward Purcell in 1946 (Bloch et al., 1946, Purcell et al., 1946). NMR originates from the interactions between microscopic nuclear magnetic moments and externally applied magnetic fields. For a nucleus to have a magnetic moment, it must have a net angular momentum and charge. Spin is a fundamental property of sub-atomic particles like the nucleus. Nuclear spin is analogous to angular momentum at the quantum level and is described by integer or half integer (½, 1, 3/2 …) values of a discrete quantized amount of angular momentum. Protons and electrons each have a spin of ½ and are either positively or negatively charged (Keevil, 2001), thus they poses a magnetic moment and can produce NMR signals. For the purpose of introducing MRI in this thesis, the focus will be on hydrogen nuclei. The

nucleus of the hydrogen atom, consisting of a single proton, is the target of MRI because of its high NMR sensitivity and because of its abundance in the body.

When a group of nuclei is placed in an external magnetic field (B0) the magnetic moments of the nuclei will align either parallel or anti-parallel to the field (Figure 1.1). In equilibrium, the net magnetic moments or magnetization occurs only along the longitudinal axis, or z-axis (direction of the constant magnetic field). This is because the parallel alignment is at a lower energy state and thus has a higher probability of being populated.

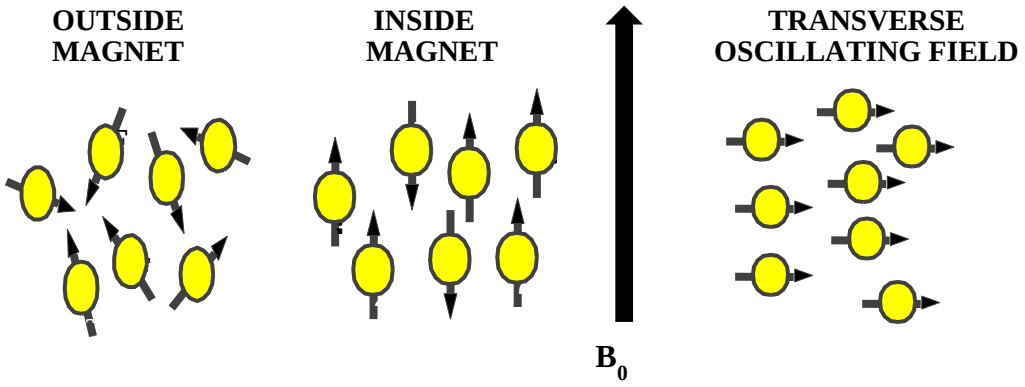

Figure 1.1: Magnetic moments (small arrows) of the nuclei (circles) are aligned randomly when outside a strong magnetic field. When placed in an external magnetic field (B0), nuclei align parallel and anti-parallel to the field. The magnetization is then displaced by applying a transverse oscillating field.

The magnetization can be displaced away from the z-axis by the application of a transverse oscillating magnetic field (B1) at a specific frequency (Figure 1.1). Any magnetization that is in the transverse plane will oscillate or precess about the z-axis due to the interaction with the B0 field. The frequency of this precession is directly proportional to the B0 field at that location and is called the Larmor frequency. This

oscillating magnetization induces current in the MRI receiver coil and this is the oscillating transverse magnetization that gives rise to the signal that is detected by MRI. The frequency range of MRI signals is near that of radio receivers (10 - 900 Mhz) and is said to be at radio frequencies (RF). By adding linear magnetic field gradients, multiple Larmor frequencies are produced that encode the spatial locations of the nuclei. The signal becomes a mixture of frequencies that are mathematically (Fourier) transformed to produce the image (Huettel, 2009). The intensity and thus the contrast at each location in the image is dependent on the T1 and T2 relaxation.

1.1.1 T1 and T2 Relaxation

When the B1 field is turned off, the molecules begin to return to their equilibrium configuration. The transverse component decays and the longitudinal component recovers back to its original magnitude. This is known as relaxation. Relaxation is associated with redistribution of energy within the spin system and the loss of energy to the surroundings or "lattice". The time constant that describes the rate of recovery of the longitudinal component to its original position is called T1 relaxation or spin-lattice relaxation. The measure of the decay of the transverse component over time is called T2 relaxation or spin-spin relaxation. Relaxation affects the magnitude of the magnetization that is detected by a receive coil in the MRI scanner. Thus, the information gathered by the scanner is: 1) the energy release; 2) T1 relaxation; and 3) T2 relaxation (Keevil, 2001).

The maximum energy release is an estimate of the number of observable hydrogen nuclei which ultimately corresponds to the amount of water in the tissue sample. T1 and T2 relaxation times depend on the efficiency of energy exchange at the

microscopic level. The mechanism of this exchange is magnetic coupling to the spin system. Since the spin system is placed into a magnetic field and thus has an energy splitting directly proportional to the Larmor frequency, the most efficient energy exchange happens when fluctuations occur near the Larmor frequency. The nucleus can be thought of as a very sensitive probe of the dynamics of its immediate magnetic surroundings. Relaxation can be affected by chemical bonding, viscosity, molecular size and molecular motions and reflects the surroundings of each individual atom.

Using the properties of T1 and T2 relaxation, it is possible to emphasize tissues that show different characteristics in relaxation times. MR Images in which contrast is associated with differences in T1 relaxation times are called T1-weighted whereas contrast linked to differences in T2 relaxation times are called T2-weighted images.

1.1.2 Image Acquisition

1.1.2.1 T1- and T2-weighted Images

In order to achieve T1-weighted and T2-weighted images, one can use a variety of pulse sequences. In these experiments, the Spin Echo sequence was used.

The Spin Echo sequence is based on a pulse sequence consisting of a 90 degree RF pulse followed by a 180 degree RF pulse (Figure 1.2). The application of this pair of pulses, 90 followed by 180 degree, results in a spin echo forming at a time equal to the interval between the first and second pulse (Hahn, 1950). Echo time (TE) is the time between the 90 degree pulse and the time where the echo forms. The two pulses are repeated and thus the repetition time (TR) is the time between the two successive 90 degree pulses. Figure 1.2 illustrates both TE and TR times.

After excitation, the longitudinal magnetization is rotated down to the transverse (xy) plane. As the spins lose energy, the longitudinal magnetization then recovers back to its original state according to the T1 relaxation time. TR determines how much longitudinal magnetization can recover between cycles which is proportional to the T1 contrast (Huettel, 2009). During the TE, the transverse magnetization decays according to the T2 relaxation time, due to loss of coherence among the spins. TE determines how much the transverse signal decays (Huettel, 2009).

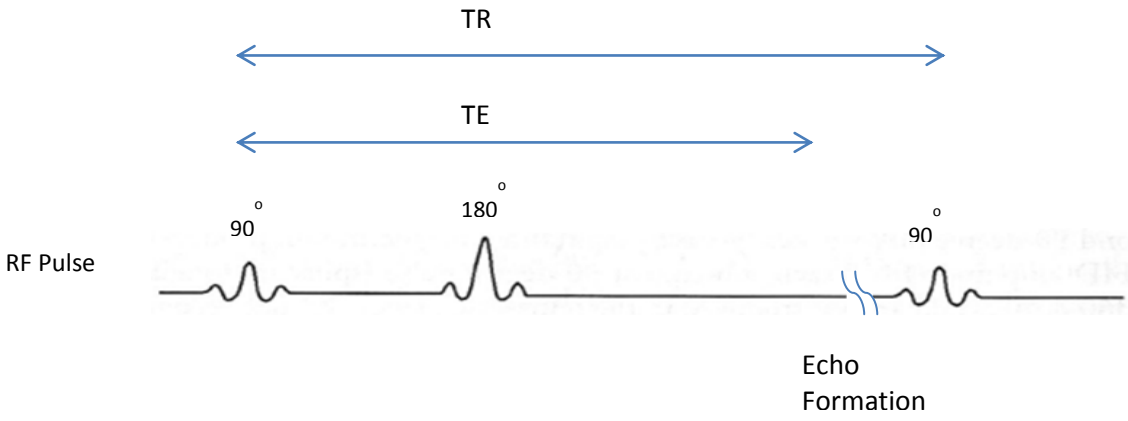

Figure 1.2: Spin-Echo Pulse sequence illustrating the TE time and the TR time with regards to the 90 degree and 180 degree pulses.

By selecting combinations of TE and TR, the contrast dependence in the image can be weighted towards T1 or T2. For a T2-weighted image, a TE usually greater than 60 ms with a long TR is used. For a T1-weighted image, a short TE and a TR less than the tissue T1s is used. General times are as follows; T1 weighted: short TE (smaller than 12 ms) and short TR (300-600 ms); T2 weighted: long TE (greater than 60 ms) and long TR (greater than 1600 ms) (Bitar et al., 2006).

1.1.2.2. T1 and T2 Mapping

The quantitative imaging approach focuses on measuring the values of the tissue relaxation properties (T1 and T2). This includes collecting a set of images from which the relaxation parameters can be calculated based on a theoretical model. Such a calculated image will be referred to as a map. Mapping provides sensitivity to the full range of T1 and T2s, and has the potential to quantify the tissue concentrations of a contrast agent. For the purpose of this thesis, the relaxivity of manganese (introduced below) in tissue is measured mainly using the mapping of T1.

T1 maps can be generated from sets of saturation recovery images with varying saturation times. The saturation time is the time between a 90 degree preparation pulse and the image acquisition. The image intensity at any location is described by Equation 1.1, where I is equal to intensity, I_0 is the equilibrium intensity, TR is the repetition time, T1 is the relaxation time and *a* is equal to 1 for 90 degree pulse and 2 for an inversion (180 degree) preparation.

$$I=I_0(1-ae^{-TR/T_1}) \qquad \text{Equation 1.1}$$

Any non-linear curve fitting procedure can be used to calculate the parameters that best match the data to the equation. This is performed for each pixel position in the data set. The calculated T1 values are displayed as gray scale intensities to make up the T1 map.

T2 maps are generated using a set of images with the same TR but multiple TE's. The image intensity is described by Equation 1.2, where TE is equal to the set of echo

times and T2 is equal to the relaxation time. Through the fitting procedure the two parameters are assigned.

$$I=I_o e^{-TE/T_2} \qquad \text{Equation 1.2}$$

1.1.3 Introduction to Paramagnetics

Paramagnetic materials (e.g. Mn^{2+}, Gd^{3+}) have unpaired electrons which result in a net magnetic moment. The longitudinal T1 relaxation time and transverse T2 relaxation time of the protons are determined by molecular motions that produce fluctuating local magnetic fields. The protons interact with each other through dipole-dipole interactions. Since the magnetic dipole produced by an electron is much stronger that that produced by the nucleus, the interaction is dominated by a dilute number of paramagnetic ions. The relaxation rates (1/relaxation times) are linearly dependent on the concentration of the paramagnetic substance.

The metal manganese, in the form of its divalent ion, Mn^{2+} (for brevity, Mn will be used for the remainder of this thesis) is paramagnetic and causes strong reduction of both T1 and T2 relaxation time constants of tissue water (Silva and Bock, 2008). The extent of T1 or T2 reduction depends on the local Mn concentration and can be described by:

$$Ri_o = Rt(0) + Ri\,[Mn^{2+}] \qquad \text{Equation 1.3}$$

Where $Ri_o = 1/Ti$ (i=1,2) is the observed relaxation rate, $[Mn^{2+}]$ is the concentration of the Mn^{2+} ion, Ri is the relaxivity constant, and Rt(0) is the relaxation rate of the solvent without manganese ($[Mn^{2+}] = 0$).

The significance of this magnetization is that some paramagnetics can be delivered to the body and used as contrast agents. This is commonly done in clinical imaging (e.g. using gadolinium for enhancing tumors of the liver, kidney etc…). The use of manganese and its unique properties as a contrast agent in MRI is known as MEMRI.

1.2 Manganese-Enhanced Magnetic Resonance Imaging (MEMRI)

The use of manganese as a contrast agent for the use in animal studies is a relatively recent advance in MRI studies. The properties, issues of toxicity, delivery routes and commonly used concentrations of manganese will first be introduced followed by an introduction to the use of MEMRI in the current literature.

1.2.1 Properties of Manganese

Manganese (Mn) is an essential heavy metal that is ubiquitous in nature. It plays important roles in the metabolism and synaptic function as an antioxidant and enzymatic cofactor in the brain (Chuang et al., 2009b). Mn is an important co-factor in a number of key enzymes, including manganese superoxide dismutase, pyruvate carboxylase and glutamine synthetase (Silva and Bock, 2008).

However, while Mn in trace amounts is an essential ion for normal cellular functioning, chronic overexposure to the metal can lead to a progressive and permanent neurodegenerative disorder in humans and nonhuman primates called “manganism”

(Roth, 2006). Manganism resembles the main pathological features of Parkinson's disease (Silva and Bock, 2008). Excess Mn damages the central nervous system by a number of mechanisms, including inhibition of mitrochondrial oxidative phosphorylation (Chuang et al., 2009b). In addition to the deleterious effects of chronic overexposure, acute overexposure to Mn (such as by injection of Mn substance systemically in an experimental model) can also lead to hepatic failure and cardiac toxicity (Silva and Bock, 2008).

The simplest way to administer of Mn is to use a $MnCl_2$ solution (Silva and Bock, 2008). According to the Material Safety Data Sheet (MSDS) for $MnCl_2$, the target organs include the central nervous system and the lungs, and characteristic signs and symptoms of exposure have been identified. Silva et al., 2004 states that 'men exposed to manganese dusts showed a decrease in fertility with early symptoms including languor, sleepiness and weakness in the legs.' Regardless of these toxicity issues, researchers continue to find ways of avoiding Mn's toxic effects so that they can benefit from its paramagnetic properties.

In order to reduce some of the toxic effects of manganese, researchers must also take into consideration the osmolarity and the pH of the solution which should be biocompatible with the organism or tissue of interest. The osmolarity of most extracellular body fluids is about 300 mOsm. Because $MnCl_2$ consists of 3 ions, a 100 mM $MnCl_2$ solution would result in an isotonic solution. Unbuffered aqueous solutions of $MnCl_2$ are slightly acidic. Thus, the pH of $MnCl_2$ needs to be controlled by adjustment to values near 7.4 using sodium hydroxide or by preparing manganese solutions with a buffer such as bicine or Tris-HCL (Seo et al., 2011a).

Toxicokinetic parameters such as half-lives, uptake times and clearance rates have recently been studied (Zheng et al., 2000). Along with the methods above, considering these parameters can also help in determining a less toxic dosing regime for MEMRI. It has been shown that there is a long half-life of manganese in the brain (51–74 days) relative to its short half-life in visceral organs like the heart and the liver (Takeda et al., 1995). It was also found that when injected systemically Mn has a total body (not including brain) clearance rate of 0.43 L/h/kg and a blood terminal elimination of 1.83 h (Zheng et al., 2000). Taking this into consideration, it has been proposed to apply $MnCl_2$ in a fractionated manner (i.e. smaller doses more often) to reach a sufficient Mn accumulation while minimizing toxic side effects (Takeda et al., 1995; Bock et al., 2008).

The issues of $MnCl_2$ toxicity requires a compromise between avoiding toxicity and delivering adequate amounts of manganese for MEMRI (Silva and Bock, 2008). The goal of optimizing MEMRI signal enhancement and strategies for efficient delivery of Mn to the brain, while minimizing toxicity to the animal creates the question of the optimum methodology to use in MEMRI experiments (Silva et al., 2004).

Questions regarding the most efficient route of administration and the most effective concentration to use have yet to be answered. Below, I will summarize some common delivery routes and concentrations described in the current literature.

1.2.2 Manganese Delivery Routes

In order to increase the successful application of MEMRI, the delivery of Mn to the site of interest must be considered. In animals, Mn can be injected intravenously (IV), subcutaneously (SQ), intraperitoneally (IP) or as an injection directly into the area of

interest (i.e. the brain). The simplest way to deliver Mn is to inject a solution of the salt $MnCl_2$ (Silva and Bock, 2008). After injection, $MnCl_2$ dissociates into Mn^{2+} and Cl^-.

The routes of delivery, systemic or local cerebral administration, are applied for different reasons: 1) systemic administration which reaches the brain via the blood, enhances cerebral cytoarchitecture that would otherwise be difficult to reveal as well as to demarcate active regions of the brain; and 2) local cerebral administration enables one to map neuronal tracts in the living brain where Mn is stored and transported along axonal tracts (Bouilleret et al., 2011).

1.2.2.1 Systemic Administration

The earliest work with Mn as an MRI contrast agent relied on giving a systemic dose of $MnCl_2$ and monitoring distribution in a number of tissues. It was discovered that Mn accumulates in almost all tissues when administered systemically (Kang and Gore, 1984). One study investigated the relative MRI enhancement obtained with different systemic routes of administration (SQ, IP) and concluded that both the temporal and regional changes in cerebral T1 relaxation following $MnCl_2$ infusion are relatively independent of the route of administration (Kuo et al., 2005).

Systemic application of Mn leads to an accumulation in specific brain areas including the basal ganglia, hippocampus, pituitary gland, cerebellum and olfactory bulb (Silva et al., 2004). The tissue-specific accumulation of Mn is dependent on the cerebral spinal fluid (CSF)-brain transport mechanisms from the lateral ventricles leading to a facilitated uptake in adjacent areas (Bock et al., 2008a). Also, it has been shown that the distribution of manganese may reflect the density of astrocytes (Henriksson et al., 2000),

neurons (Paulter et al., 1998), or mitochondria (Akai et al., 1990, Gavin et al., 1990). It is known that Mn ions cannot passively enter the brain parenchyma through an intact blood brain barrier (BBB) (Aoki et al., 2004a). Mn, however, can slowly diffuse into brain parenchyma via the blood-CSF barrier (BCB) present at the choroid plexus in ventricles (Aoki et al., 2004a). This distribution of manganese eventually leads to enhancement in multiple brain regions.

One downfall of using a systemic Mn injection is that before it reaches the brain, it is absorbed by the liver, heart and kidneys. This can cause many acute toxic effects including compromised cardiovascular function, renal failure and liver failure. This is why, is some cases, it is safer to use an administration of Mn focally as it could reduce some of these toxic effects.

1.2.2.2 Local Injection

For a more direct administration, focal injections are often used to target areas of interest, primarily in the brain. A range of recent studies have used direct injections of Mn to trace neuronal connections in rodents (Table 1.1). Due to the fact that Mn is a calcium (Ca^{2+}) analogue, in the CNS, Mn can enter excitable cells via voltage-gated Ca^{2+} channels, the sodium (Na^{+})/Ca^{2+} exchanger, the Na^{2+}/ magnesium (Mg^{2+}) antiporter and the active Ca^{2+} uniporter in mitochondria (Paulter, 1998). Once inside cells, some Mn is packaged in the endoplasmic reticulum and is transported anterogradely along microtubules in axonal tracts (Pautler, 2006) . Upon reaching the presynaptic membrane, it is released into the synaptic cleft along with the neurotransmitter glutamate (Silva and Bock, 2008).

As stated above, focal injections are beneficial as the issue of toxicity is less severe in MEMRI experiments that use a local injection of $MnCl_2$ in the brain because there is little exposure to Mn outside of the injection site (as opposed to systemic circulation) and immediately adjacent areas. It also allows for a marked reduction of the total amount of applied manganese.

1.2.3 Concentrations of $MnCl_2$ Solutions

A systemic dose ranging from 9-175 mg/kg, either in one bolus injection or multiple injections (Table 1), have been used in MEMRI. This wide range of doses leads to MRI detection of the basal ganglia, hippocampus, pituitary gland, cerebellum and olfactory bulb (Silva et al., 2004). Contrast enhancement increases with increasing doses of $MnCl_2$. In general both the contrast as well as the signal intensity of the enhanced regions are increased, allowing for better distinction of anatomical features (Silva et al., 2004). In focal injections, concentrations ranging from 2-9 mg/kg (Table 1) lead to MRI detection in the areas of interest.

The MSDS for $MnCl_2$ shows that acute systemic doses as low as 93 mg/kg in rats have significant adverse effects including high mortality rates. However, recent MEMRI experiments (Table 1.1) have safely used similar doses, or even higher doses, with manageable or no adverse effects. Unfortunately, MRI studies do not necessarily include a formal behavioural test and the assessment of potential toxic effects are usually limited to a "subjective general observation" of animal behavior in the home cage (Eschenko et al., 2010b). Also, it is unlikely, that animal models of brain disease will tolerate these high doses. Additionally, in studies which concern the use of behavioural or neurological

testing, high concentrations may affect behavioural outcomes and thus may not be ideal for *in vivo* studies. High doses are also not advisable for longitudinal studies which require repeated injections (Silva and Bock, 2008). In these cases, research groups have begun to use (and recommend – Eschenko et al., 2010b) a slow release delivery system achieved with the use of an osmotic pump.

Table 1.1: Summary of injection routes and doses, ordered by method of injection.

Reference:	Concentration in mg/kg	Concentration in mM	Method of Injection
Lin and Koretsky (1997)	54 mg/kg		Intravenous
Aoki et al. (2004c)	175 mg/kg		Intravenous
Cross et al. (2009)	75 mg/kg		Tail Vein
Chuang et al. (2009a)	175 mg/kg		Tail Vein
de Sousa et al. (2007)	175 mg/kg		Tail Vein
Aoki et al. (2002)	53 mg/kg		Intra-arterial
(Inui-Yamamoto et al., 2010)	20 mg/kg		Intra-peritoneal
Tambalo et al. (2009)		270 mM 0.2 mmol/kg	Intra-peritoneal
Jackson et al. (2011)	40 mg/kg		Intra-peritoneal
Bouilleret et al. (2011)	100 mg/kg		Intra-peritoneal
Eschenko et al. (2010a)	16 mg/kg –32 mg/kg – 80 mg/kg		Subcutaneous
Eschenko et al. (2010b)	16 mg/kg 80 mg/kg		Subcutaneous
McCreary 2011	7.14 mg/kg		Lateral Ventricle
Seo et al. (2011a)	7.14 mg/kg	100 mM 2 mM rate 180 µL/kg/hr	Left Lateral Ventricle
Seo et al. (2011b)		0.1 umol/h	Left lateral ventricle
van der Zijden et al. (2008)		0.2 uL 1 mol/L 0.05 uL/min	Sensorimotor cortex
Yang et al. (2011)		120 mmol/L	Right medial thalamus
Sandvig et al. (2011)		3 uL of 150 nmol	Intravitreal

1.2.4 Use of Osmotic Pumps to Deliver Manganese

Some research groups have started to use slow release mechanisms such as the osmotic pump to deliver Mn (Canals et al., 2008, Eschenko et al., 2010a). The use of osmotic pumps to deliver a specific concentration of Mn over a specified period of time could decrease many of the toxicity issues which one must face when dealing with MEMRI experiments. In some cases, an osmotic pump enables an increase in Mn concentration (and therefore a greater Signal to Noise Ratio [SNR]) while keeping the toxicity of the ion to a minimum. Canals et al. (2008) demonstrated that Mn doses that resulted in dramatic cortical lesions when injected acutely into the brain parenchyma, can safely be applied to the brain when delivered at a constant and slow infusion rate (Canals et al., 2008) . The present experiments use the ALZET ® (Alzet, Durect) osmotic pump (Figure 1.3).

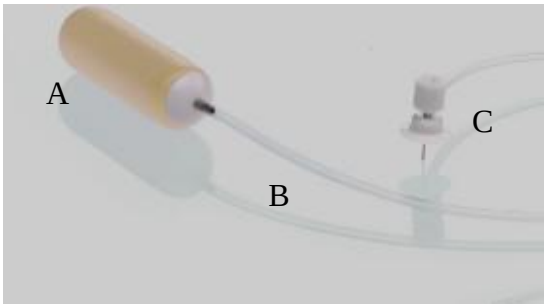

Figure 1.3: ALZET pump (A) attached to a vinyl catheter (B) connected to a cannula (C). Flow moderator (inside pump) controls the amount of solution delivered from the pump to the cannula or external environment. Osmotic pump is inserted subcutaneously whereas a cannula, for focal injections can be implanted to the brain region of interest.

ALZET pumps operate due to an osmotic pressure difference between a compartment within the pump, and the tissue environment in which the pump is

implanted. As water enters from the body into the pump compartment, it compresses the flexible reservoir, displacing the $MnCl_2$ solution from the pump at a controlled, predetermined rate. ALZET provides a variety of delivery rates, and these pumps can administer the solution in the same fashion as a syringe (SQ or IP implant, cannulation to brain) (Theeuwes and Yum, 1976).

1.2.5 The Use of MEMRI in Neuroscientific Studies

MEMRI with systemically injected $MnCl_2$ has proven to be a promising technique for brain imaging in live animals. There are several features that suggest that Mn infusion is uniquely suited for brain imaging (Eschenko et al., 2001).

Divalent Mn is paramagnetic and reduces the T1 relaxation times of water protons. This feature enhances specific cytoarchitectural characteristics using Mn as a contrast agent. Many studies have benefited from this technique as they are able to detect specific neuroarchitectonic features in the rodent brain using MRI after systemic $MnCl_2$ administration (Lin and Koretsky., 1997, Aoki et al., 2004b, de Sousa et al., 2007, Jackson et al., 2011). One study showed the development of the rat brain and measured T1 at several stages of rat brain development in the presence of Mn (de Sousa et al., 2007). Another study compared the uptake of Mn in a marmoset brain versus a rat brain and found differences in the structures which had the highest enhancement (Bock et al., 2008). Most recently, Jackson et al. (2011) used Mn to study hippocampal structure and function in parallel with cognitive testing. They applied behavioural testing to investigate if the Mn disrupted hippocampus-dependent behaviour and found that it did not have adverse effects on behaviour (Jackson et al., 2011).

Secondly, Mn can reflect anatomical connectivity as it is taken up by cells and anterogradely transported along neural pathways. In 1998, Paulter and colleagues utilized the paramagnetic properties of Mn, performing the first *in vivo* Mn tract tracing experiment (Pautler et al., 1998) . They showed that administration of $MnCl_2$ into the rat and mice olfactory receptor neurons leads to contrast enhancement in the olfactory bulb and primary olfactory cortex in MRI. Since this first experiment, MEMRI has been used to trace several pathways including the visual optic tract in rats (Murayama et al., 2006), olfactory tract in rats (Cross et al., 2004) and hippocampal pathways in rats, mice and monkeys (Watanabe et al., 2001, Chen et al., 2007) as well as the song center in birds (Van der Linden et al., 2009).

Finally, Mn is transferred through voltage-gated channels to neurons at fairly low rates and therefore its accumulation is relatively proportional to neural activity. For this reason, Van der Linden et al. (2007) reported that activation in awake moving animals can be monitored by performing MRI after the presumed activity has occurred, when preceded by an intraperitoneal injection of Mn. Mn will accumulate in activated areas of the brain, and MEMRI can be used to investigate such areas after an external stimulation. For example, stimulation of whisker barrels in rats shows a clear relationship between manganese-enhanced cortical regions and whisker tactile-sensory-evoked activity (Weng et al., 2007). Yet another study used MEMRI to map the auditory brainstem in mice (Yu et al., 2005).

MEMRI has been used in previous studies. Nevertheless, although previous studies highlight the potential of MEMRI for brain imaging, the limitations and

boundaries concerning the use of Mn in living animals and its applications in behavioural neuroscience are only beginning to be characterized.

1.3 Thesis Objectives and Rationale

The main objective of the thesis is to apply MEMRI to studies in neuroscience by first establishing the limitations concerning the use of MEMRI in live rats.

The major objectives of this thesis include:

1) Develop an MEMRI protocol in rats for direct injection of Mn into the lateral ventricle using a cannula and an implanted osmotic pump system.
2) Determine the neurotoxicity of Mn using an array of behavioural tests.
3) Optimize the Mn application procedure to reduce neurotoxic effects.
4) Apply MEMRI to a filial generation of stressed rats using subcutaneously implanted osmotic pumps for systemic Mn administration.
5) Compare the resolution of MEMRI recordings to histology in experiments using systemic and intraventricular injections.

The present thesis is structured into three chapters. Chapter 2 assesses the intraventricular cannulation of Mn and Chapter 3 assesses the use of MEMRI as a tool to analyze prenatally stressed rats. The experimental chapters are followed by a final discussion and conclusions chapter.

1.4 References

Aoki I, Naruse S, Tanaka C (2004a) Manganese-enhanced magnetic resonance imaging (MEMRI) of brain activity and applications to early detection of brain ischemia. Nmr in Biomedicine 17:569-580.

Aoki I, Wu YJL, Silva AC, Lynch RM, Koretsky AP (2004b) In vivo detection of neuroarchitecture in the rodent brain using manganese-enhanced MRI. Neuroimage 22:1046-1059.

Bitar R, Leung G, Perng R, Tadros S, Moody AR, Sarrazin J, McGregor C, Christakis M, Symons S, Nelson A, Roberts TP (2006) MR pulse sequences: what every radiologist wants to know but is afraid to ask. Radiographics : a review publication of the Radiological Society of North America, Inc 26:513-537.

Bloch F, Hansen WW, Packard M (1946) The Nuclear Induction Experiment. Phys Rev 70:474-485.

Bock NA, Paiva FF, Nascimento GC, Newman JD, Silva AC (2008) Cerebrospinal fluid to brain transport of manganese in a non-human primate revealed by MRI. Brain research 1198:160-170.

Bouilleret V, Cardamone L, Liu C, Koe AS, Fang K, Williams JP, Myers DE, O'Brien TJ, Jones NC (2011) Confounding Neurodegenerative Effects of Manganese for In Vivo MR Imaging in Rat Models of Brain Insults. Journal of Magnetic Resonance Imaging 34:774-784.

Canals S, Beyerlein M, Keller AL, Murayama Y, Logothetis NK (2008) Magnetic resonance imaging of cortical connectivity in vivo. Neuroimage 40:458-472.

Chen W, Tenney J, Kulkarni P, King JA (2007) Imaging unconditioned fear response with manganese-enhanced MRI (MEMRI). Neuroimage 37:221-229.

Chuang K-H, Koretsky AP, Sotak CH (2009a) Temporal Changes in the T1 and T2 Relaxation Rates (R1 and R2) in the Rat Brain Are Consistent With the Tissue-Clearance Rates of Elemental Manganese. Magnetic Resonance in Medicine 61:5.

Chuang KH, Koretsky AP, Sotak CH (2009b) Temporal changes in the T1 and T2 relaxation rates (DeltaR1 and DeltaR2) in the rat brain are consistent with the tissue-clearance rates of elemental manganese. Magnetic resonance in medicine : official journal of the Society of Magnetic Resonance in Medicine / Society of Magnetic Resonance in Medicine 61:1528-1532.

Cross DJ, Minoshima S, Anzai Y, Flexman JA, Keogh BP, Kim YM, Maravilla KR (2004) Statistical mapping of functional olfactory connections of the rat brain in vivo. Neuroimage 23:1326-1335.

Cross AR, Alaverdashvilli M, Lapointe V, Whishaw I.Q (2009) MEMRI and Single Pellet Reaching in Rats. Conference Proceedings, ISMRM, Hawaii

de Sousa PL, de Souza SL, Silva AC, de Souza RE, de Castro RM (2007) Manganese-enhanced magnetic resonance imaging (MEMRI) of rat brain after systemic administration of MnCl2: changes in T-1 relaxation times during postnatal development. Journal of Magnetic Resonance Imaging 25:32-38.

Eschenko O, Canals S, Simanova I, Beyerlein M, Murayama Y, Logothetis NK (2010a) Mapping of functional brain activity in freely behaving rats during voluntary running using manganese-enhanced MRI: Implication for longitudinal studies. Neuroimage 49:2544-2555.

Eschenko O, Canals S, Simanova I, Logothetis NK (2010b) Behavioral, electrophysiological and histopathological consequences of systemic manganese administration in MEMRI. Magnetic Resonance Imaging 28:1165-1174.

Hahn EL (1950) Spin Echoes. Phys Rev 80:580-594.

Huettel SA, Song, Allen W., Mccarthy Gregory (2009) Functional Magnetic Resonance Imaging. 23 Plumtree road, Sunderland, M.A. USA: Sinauer associates, Inc.

Inui-Yamamoto C, Yoshioka Y, Inui T, Sasaki KS, Ooi Y, Ueda K, Seiyama A, Ohzawa I (2010) The brain mapping of the retreival of conditioned taste aversion memory using manganese-enhanced magnetic resonance imaging in rats Neuroscience 167:199-204.

Jackson SJ, Hussey R, Jansen MA, Merrifield GD, Marshall I, MacLullich A, Yau JL, Bast T (2011) Manganese-enhanced magnetic resonance imaging (MEMRI) of rat brain after systemic administration of MnCl(2): hippocampal signal enhancement without disruption of hippocampus-dependent behavior. Behav Brain Res 216:293-300.

Kang YS, Gore JC (1984) Studies of tissue NMR relaxation enhancement by manganese. Dose and time dependences. Investigative radiology 19:399-407.

Keevil SF (2001) Magnetic Resonance imaging in medicine. Physics education 36:9.

Kuo YT, Herlihy AH, So PW, Bhakoo KK, Bell JD (2005) In vivo measurements of T1 relaxation times in mouse brain associated with different modes of systemic administration of manganese chloride. Journal of Magnetic Resonance Imaging 21:334-339.

Lin YJ, Koretsky AP (1997) Manganese ion enhances T-1-weighted MRI during brain activation: An approach to direct imaging of brain function. Magnetic Resonance in Medicine 38:378-388.

Murayama Y, Weber B, Saleem KS, Augath M, Logothetis NK (2006) Tracing neural circuits in vivo with Mn-enhanced MRI. Magn Reson Imaging 24:349-358.

Pautler RG (2006) Biological applications of manganese-enhanced magnetic resonance imaging In: Magnetic Resonance Imaging: Methods and biological applications vol. 124 (Pottumarthi, P. V., ed), p 28 Totowa, New Jersey: Humana Press.

Pautler RG, Silva AC, Koretsky AP (1998) In vivo neuronal tract tracing using manganese-enhanced magnetic resonance imaging. Magnetic Resonance in Medicine 40:740-748.

Purcell EM, Torrey HC, Pound RV (1946) Resonance Absorption by Nuclear Magnetic Moments in a Solid. Phys Rev 69:37-38.

Roth JA (2006) Homeostatic and toxic mechanisms regulating manganese uptake, retention, and elimination. Biological research 39:45-57.

Sandvig A, Sandvig I, Berry M, Olsen O, Pedersen TB, Brekken C, Thuen M (2011) Axonal Tracing of the Normal and Regenerating Visual Pathway of Mouse, Rat, Frog, and Fish Using Manganese-Enhanced MRI (MEMRI). Journal of Magnetic Resonance Imaging 34:670-675.

Seo Y, Satoh K, Watanabe K, Morita H, Takamata A, Ogino T, Murakami M (2011a) Mn-bicine: A Low Affinity Chelate for Manganese Ion Enhanced MRI. Magnetic Resonance in Medicine 65:1005-1012.

Seo Y, Takamata A, Ogino T, Morita H, Murakami M (2011b) Lateral diffusion of manganese in the rat brain determined by T(1) relaxation time measured by (1)H MRI. Journal of Physiological Sciences 61:259-266.

Silva AC, Bock NA (2008) Manganese-enhanced MRI: An exceptional tool in translational neuroimaging. Schizophrenia Bulletin 34:595-604.

Silva AC, Lee JH, Aoki I, Koretsky AP (2004) Manganese-enhanced magnetic resonance imaging (MEMRI): methodological and practical considerations. NMR Biomed 17:532-543.

Tambalo S, Daducci A, Fiorini S, Boschi F, Mariani M, Marinone M, Sbarbati A, Marzola P (2009) Experimental Protocol for Activation-Induced Manganese-Enhanced MRI (AIM-MRI) Based on Quantitative Determination of Mn Content in Rat Brain by Fast T-1 Mapping. Magnetic Resonance in Medicine 62:1080-1084.

Theeuwes F, Yum SI (1976) Principles of the design and operation of generic osmotic pumps for the delivery of semisolid or liquid drug formulations. Annals of biomedical engineering 4:343-353.

Van der Linden A, Van Meir V, Boumans T, Poirier C, Balthazart J (2009) MRI in small brains displaying extensive plasticity. Trends in Neurosciences 32:257-266.

van der Zijden JP, Bouts M, Roeling TAP, Bleys R, van der Toorn A, Dijkhuizen RM (2008) Manganese-enhanced MRI of brain plasticity in relation to functional recovery after experimental stroke. Journal of Cerebral Blood Flow and Metabolism 28:832-840.

Watanabe T, Michaelis T, Frahm J (2001) Mapping of retinal projections in the living rat using high-resolution 3D gradient-echo MRI with Mn2+-induced contrast. Magnetic Resonance in Medicine 46:424-429.

Weng JC, Chen JH, Yang PF, Tseng WYI (2007) Functional mapping of rat barrel activation following whisker stimulation using activity-induced manganese-dependent contrast. Neuroimage 36:1179-1188.

Yang PF, Chen DY, Hu JW, Chen JH, Yen CT (2011) Functional tracing of medial nociceptive pathways using activity-dependent manganese-enhanced MRI. Pain 152:194-203.

Yu X, Wadghiri YZ, Sanes DH, Turnbull DH (2005) In vivo auditory brain mapping in mice with Mn-enhanced MRI. Nature neuroscience 8:961-968.

CHAPTER 2

Experiment 1: Intracerebroventricular Infusion of Manganese via Osmotic Pump

2.1 Abstract

Toxic effects due to high doses of Mn may confound behavioural and morphological investigations in studies using MEMRI. In this study a method of manganese administration via an osmotic pump connected to a focal cannula was used. These methods were combined in order to reduce the neurotoxic effects of Mn. The result of this study demonstrates the successful application of the intracerbroventricular cannula and osmotic pump system to administer Mn to the rat brain. Results indicate that a concentration of 0.85 mM delivered over 7 days is sufficient to produce MRI-detectable levels of Mn, similar to high systemic doses, without causing adverse toxic effects. From my knowledge, this is the first approach using an osmotic pump for Mn delivery to the lateral ventricles for acquisition of anatomical images using MEMRI.

2.2 Introduction

Since the late 1990's when Lin and Koretsky (1997) first introduced the technique of MEMRI, numerous studies have used and modified this technique. In spite of the recent increase in the number of MEMRI studies, there is no consistent method to administer Mn. Researchers use varying concentrations and different methods of administration. Inconsistent use of methods complicates the ability to compare results. More specifically, there is little consensus among investigators on safe Mn usage in animals and Mn concentrations varies between studies (Eschenko et al., 2010a). The correct administration of MEMRI requires the development of a protocol that minimizes

toxic effects of Mn (Canals et al., 2008). This is especially important when the scientific question relies on behavioural analysis. Investigators need to ensure that any deficiencies or abnormalities that they see in behaviour are not caused by Mn toxicity.

Various strategies have been used to reduce the toxic effects of Mn. The first being a focal injection directly to the target or area of interest in the rat brain to reduce the amount of Mn required (Silva and Bock, 2008). The second strategy is the use of an osmotic pump to slowly increase the concentration of Mn delivered to the rat brain (Eschenko et al., 2010a).

2.2.1 Focal Injection to the Lateral Ventricle

Recent studies have shown that focal injections are beneficial as the issue of toxicity is less severe (Silva and Bock, 2008). The benefit of using a direct injection to the target area (brain) is two-fold. First, the Mn bypasses the systemic system and therefore causes fewer complications (e.g., toxicity in heart, liver, kidneys). Second, a lower concentration is sufficient to enhance MRI signal in target regions. The intracerebroventricular infusion of Mn is one of several useful focal injection techniques employed to minimize the dosage of Mn. The infusion of Mn to combine with the cerebrospinal fluid (CSF) allows transfer to the interstitial space of the brain through the ependymal layer that covers the surface of the ventricle. Thus, a higher Mn uptake in the brain structures adjacent to the ventricles is achieved (Bock et al., 2008, Seo et al., 2011b). The diffusion of Mn through the brain tissue and active anterograde transport of Mn along pathways enables a focal injection technique, more commonly used for tract tracing, to become an application for the visualization of brain anatomy and high

resolution mapping in areas such as the hippocampus, pituitary and the basal ganglia, which can be comparable to systemic techniques.

2.2.2 Osmotic Pump

Another way to decrease Mn toxicity while keeping MRI-detectable levels of the ion is to avoid acute accumulation of high Mn concentrations by slowly infusing larger volumes using osmotic pumps (Canals et al., 2008, Sepulveda et al., 2012). In contrast to a single systemic injection, Mn administration via osmotic pumps allows a reduction in acute toxic effects, while achieving cumulative concentrations of Mn sufficient for MRI-detection (Eschenko et al., 2010a).

Combining these two techniques, an intracerebroventricular cannula attached to an osmotic pump, allows usage of an ample Mn concentration while reducing the toxic effects from systemic administration and those seen after bolus injections. The behavioural concerns of administering Mn via osmotic pumps has only recently been investigated (Eschenko et al., 2010a). This study administered Mn via an IP pump and found no effect in running wheel behaviour. To my knowledge, however, behavioural consequences of Mn infusion have not been studied when using a pump for focal administration to the lateral ventricles.

2.2.3 Objectives

This study investigates two methods of reducing Mn toxicity while comparing the effects of high and low doses. This experiment had four objectives.

1) Establishment of an MEMRI protocol in rats for direct injection of Mn into the lateral ventricle using a cannula and osmotic pump system;

2) Compare a high dose, long duration to a low dose, short duration administration;
3) Optimize the Mn application procedure to reduce toxic effects;
4) Assess the toxicity of Mn with the use of a behavioural test and histological inspection of the respective brain tissue.

2.3 Materials and Methods

2.3.1 Subjects and Housing

Four Long-Evans female rats (160 days old and weighing 350-500g) raised at the University of Lethbridge vivarium were used in this study. The animals were housed in pairs under a 12 hr light/day cycle with lights on at 7:30 AM. Animals had access to food and water *ad libitum*, except during the single pellet reaching task, in which animals were placed on a restricted diet while maintaining 85% of their baseline body weight. All procedures were performed in accordance with the guidelines of the Canadian Council for Animal Care at the University of Lethbridge.

2.3.2 Treatment

Bicine buffered Mn or bicine as a control was delivered via an osmotic pump (ALZET, California). Bicine was used instead of other buffers because it causes less toxicity issues (Seo et al., 2011a). Table 2.1 summarizes the treatment administered to each rat.

Table 2.1 Solution, concentration, duration and rate of administration for each rat.

Rat Number	Solution	Pump Duration	Concentration	Flux Rate
#150	Mn	28 days	100mM 0.25 µl/hr 200ul	3.125 µg/hr
#152	Control	28 days	100mM 0.25 µl/hr 200ul	
#151	Control	7 days	0.85mM 1 µl/hr 200ul	0.10625 µg/hr
#154	Mn	7 days	0.85mM 1 µl/hr 200ul	

***flux rate is defined as the amount or flow of Mn per unit time*

2.3.3 Surgical Procedures

The rats were anesthetized with 5% isoflurane gas in oxygen flowing at 2 l/min. When deeply anesthetized (showing no reflex to a pinch of the toe) the isoflurane gas was decreased to 2%. Breathing of the animal was monitored throughout the length of the surgery. The rats were injected with 0.03 mg/kg buprenorphine (Shering-Plough, CAN) prior to making the first incision. The incision site was also injected with 0.1 ml of 2% lidocaine and epinephrine solution (Bimeda-MTC, CAN) to reduce bleeding and maintain analgesia. Left or right lateral ventricle (depending on handedness, i.e. left handed, cannula was inserted into left hemisphere) was the target for the intracranial cannulation. Coordinates were ±2.7 mm lateral, -1.72 mm bregma and 3.7 mm ventral to skull surface. After the cannula was fixed to the skull, polyethylene tubing was connected from the cannula to the osmotic pump and was the osmotic pump was then inserted subcutaneously. Polyethylene tubing was filled with sterile saline so that Mn was not administered until after the recovery period.

It should be noted that two different methods of fixing the cannula to the skull were used. Rat 150 was treated first by Dr. David Euston and alterations were made from this surgery by Dr. Bryan Kolb. For rat 150, three nylon screws were used and the

cannula was fixed to the screws with metabond and dental acrylic. Then the screws were covered in a silicone adhesive. For rats 151, 152 and 154 a cannula was inserted and was fixed using cyanoacrylate instead of dental acrylic. In this case, sutures closed the incision over the cannula and pump.

Following surgery, the rats were injected with 1mg/kg Metacam (Boehringer Ingelheim, CAN) and kept in the surgical suite for 24 hrs for monitoring before being returned to their homecage. A 0.5 mg/kg dose of Tribrissen (Shering-Plough, CAN) was also administered twice a day for 5 days to prevent infection. Rats were given three days to recover prior to behavioural testing and imaging.

2.3.4 Behavioural Testing

Skilled Reaching Task

The single pellet reaching task was used to demonstrate the effect of Mn on fine motor skills. Animals were placed in a reaching box with a vertical slot in the front wall. Animals were trained to reach through the narrow opening to retrieve small 45 mg food pellets (BioServ Inc., USA). Pellets were placed individually into an indentation on the side contralateral to the preferred limb about 1.5 cm away from the front wall. Analysis of skilled reaching movements was performed based on protocols published earlier (Metz and Whishaw, 2000). Analysis using a three-point scale to rate fine motor movements with a rating scale with 11 movement components and 35 subcategories was conducted (see Appendix A). Percent success was calculated as an indication of rat's reaching accuracy. It was calculated as a percent of successful reaches over the total number of

pellets given (20). The rodents were pre-trained in the reaching task, injected with Mn, and tested 5 days a week until the termination of the pumps.

2.3.5 MR Imaging

Following recovery from surgery, imaging was performed (Rat 150 & 152 imaged on days 5,8,10,13,16,19,23,25& 33 days post-surgery, Rat 151 &154 imaged on days 2,4,8 &10 days post-surgery). A 4.7 T 330 mm bore Oxford magnet (Oxford, UK) and a MR5000 (SMIS, UK) console was used (Figure 2.1). A 2-RF coil system consisting of a quadrature birdcage transmit coil (10 cm in diameter, 10 cm in length; Morris Instruments, CAN), a custom-built receive-only butterfly coil (2 cm in diameter) and PIN diode switching was used. Locator images (SE-TR=700 TE=13 ms 0.2x0.2x1.5 mm) were followed by a 7-image saturation recovery (SE-TE=22, TR = 100-4000 ms 0.39x0.39x1.5 mm) T1 mapping data set. Signal intensity from regions of interest (ROIs) were extracted from the T1 images using Analyze 8.1 (BIR, USA) and T1 values were calculated using custom- written software using IDL (ITT, USA).

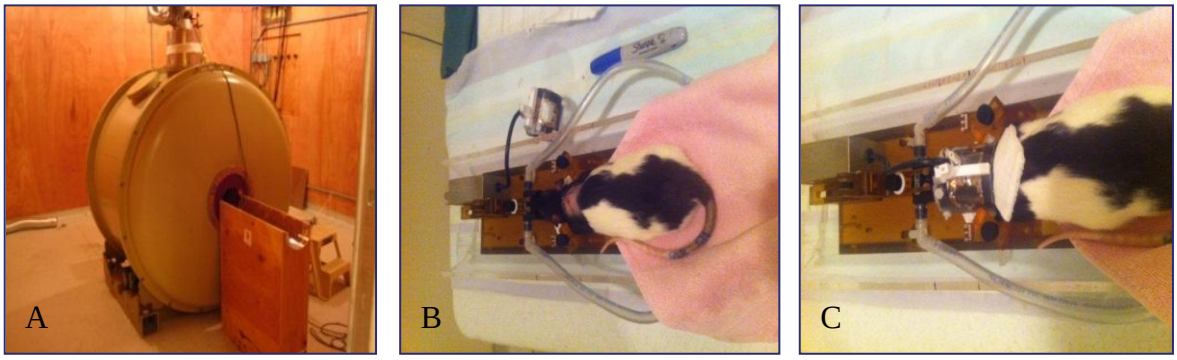

Figure 2.1: Image displaying A: The 4.7 T 330 mm bore Oxford magnet; and B: the apparatus for rat immobilization displaying the custom-built receive-only butterfly coil off the head; and C: the coil placed on the rat's head.

2.3.6 Histology

Rats were euthanized at the end of their pump durations. Rats were injected with Euthansol (Merck, CAN) and perfused transcardially with a phosphate buffer solution (PBS) followed by a trancardial injection of 4% paraformaldahyde (PFA) both with a volume of 200 mL (standard operating procedure).

Brains were extracted and sectioned coronally using a cryostat (rat #150) or microtome (rat #151,152,154) at a thickness of 40μm. Twelve series of sections were taken and stored in a 1X PBS solution with a 1:1000 concentration of sodium azide to prevent growth of bacteria or fungus. Every 3rd series was mounted on slides (VWR international, USA) dipped in 1% Gelatin and 0.2% Chromalum, and then stained with cresyl violet (for protocol, see Appendix B). The slides were captured as images using a Zeiss Axioimager M1 microscope (Zeiss, Germany).

2.4 Results

2.4.1 Analysis of T1 Relaxation Rates

All statistical computations were done using SPSS 13.0 software (IBM, USA). All graphs were created using Origin 5.0 lab freeware (Originlab, USA). T1 measurements were taken at the base of the cannula (Figure 2.2). Applications of the 28 day and 7 day pumps with Mn show an increase in T1 rate which correlates to the concentration of Mn used (Figure 2.3). Rats with the higher Mn concentration (28-day pumps) showed a larger change in T1 rate (Figure 2.3). Figure 2.3 A and B shows that the T1 rate in both controls was around 0.0007 m s^{-1}, which is equivalent to naïve rats receiving no treatment. The

28-day Mn treated rat reached a T1 rate of 0.0016 ms^{-1} whereas the 7-day Mn treated rat reached a lower rate of 0.001 ms^{-1}.

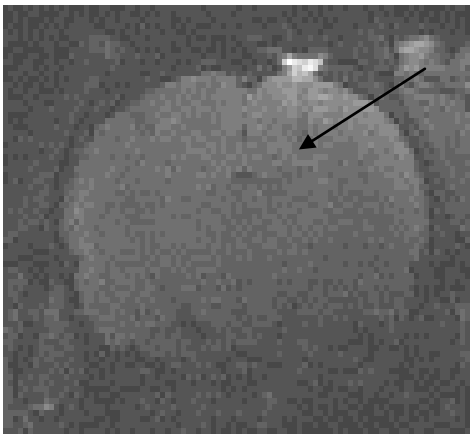

Figure 2.2: Coronal slice of the 28-day Mn subject. Arrow indicates the area of pixel analysis for T1 measurements.

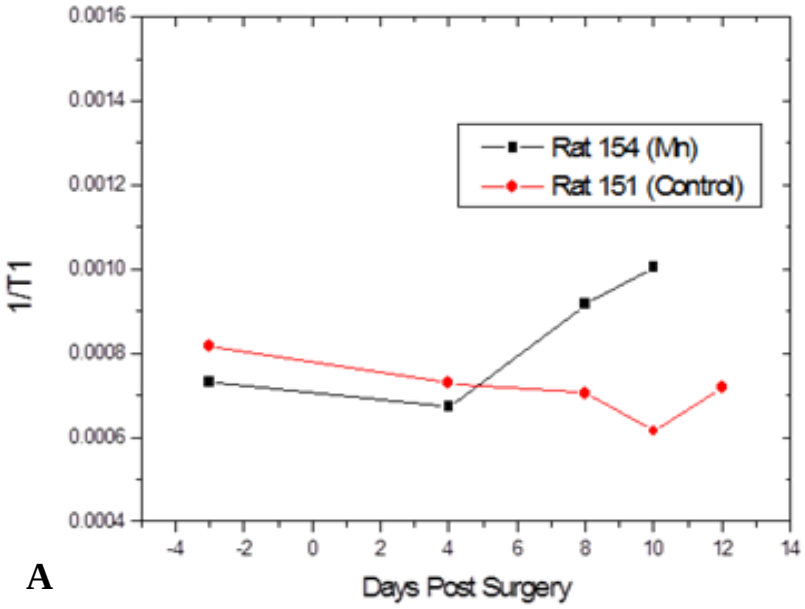

A

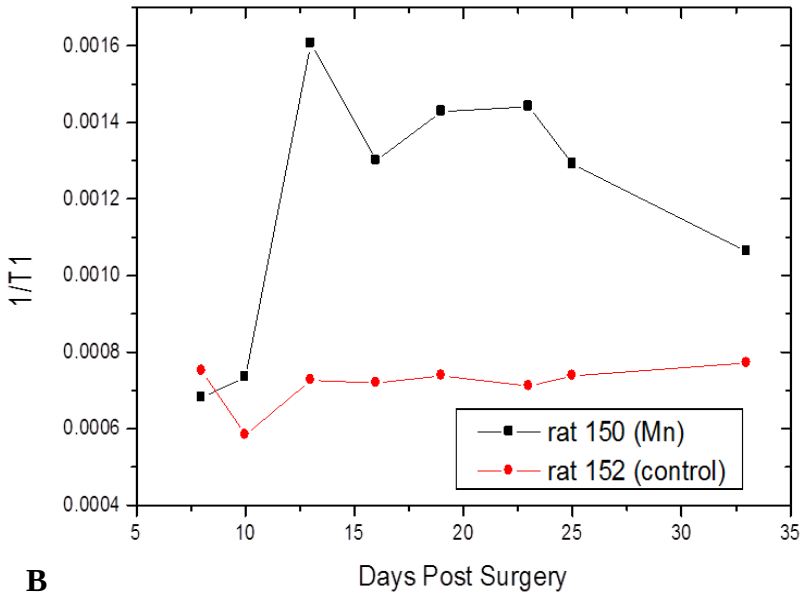

B

Figure 2.3: Time course of the 1/t1 rate (ms^{-1}) of the pixel measurements taken from under the cannula for A: 7-day subjects and B: 28-day subjects. *note, for rat 154 the last data point is absent due to technical issues that occurred with the MRI scanner.

T1 maps were created using non-linear 3-parameter curve fitting (Equation 1.1). Figures 2.4A and 2.4B show the T_1 rate maps of the 7-day Mn rat compared to the control respectively. Figures 2.4C and 2.4D show the T1 rate maps of the 28-day Mn rat compared to the control respectively. Both maps demonstrate a clear change in the T_1 values from control to Mn treatment.

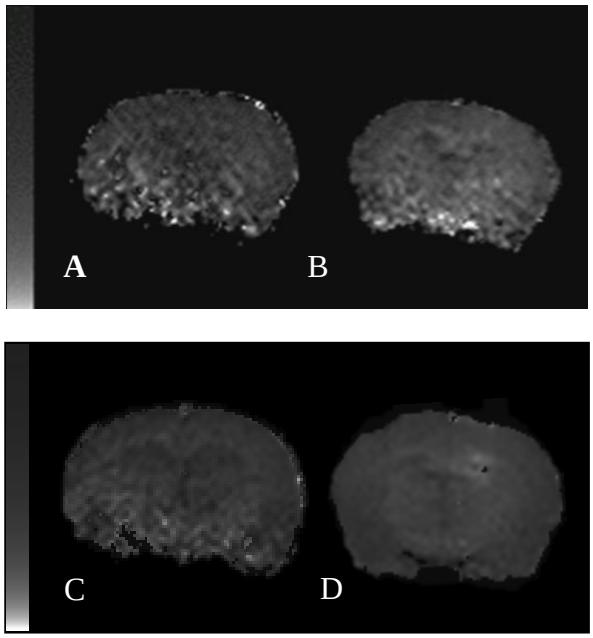

Figure 2.4: T1 rate maps for A: 7 day control B: 7-day Mn C: 28-day control D: 28-day Mn. Scale bar is 1/200 → 1/3000 ms.

Rat 150 had images of better quality and resolution due to the method of cannula fixation used (see section 2.3.3 Surgical Procedures). The cyanoacrylate method (used in rats 151, 152 & 154) caused a problem with coil placement resulting in poor image resolution. Because the cannula was only held in place with cyanoacrylate (as opposed to dental acrylic), it was precarious applying the butterfly coil directly against the rats head. This decreased the amount of signal gained in the remaining animals.

2.4.2 Signal Enhancement in Hippocampus

Signal enhancement in the hippocampus was shown in both the 28-day Mn rat and the 7-day Mn rat. Figures 2.5A and 2.5B show the progression of the enhancement in the hippocampus in the 28-day and 7-day rat respectively. Note, on day 2 of Figure 2.5B, there is an image artifact due to signal from some silicon glue on the coil which became folded into the image from outside the area of interest. Figure 2.6 shows that there was movement of Mn to the contralateral side of the brain from the cannula, which can be seen in a sagittal image.

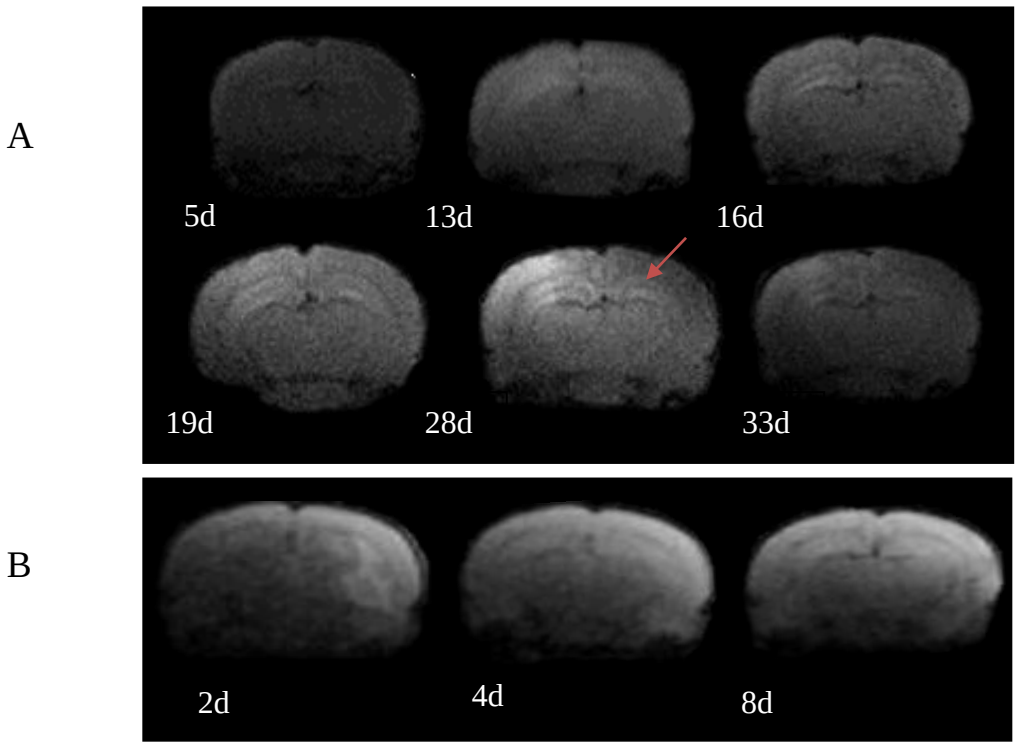

Figure 2.5: Coronal images of progression of enhancement in A: the high dose experiment, images acquired 5,13,16,19,28 and 33 days post- surgery B: low dose 2, 4, 8 days post-surgery. Red arrow is indicating the hippocampal formation.

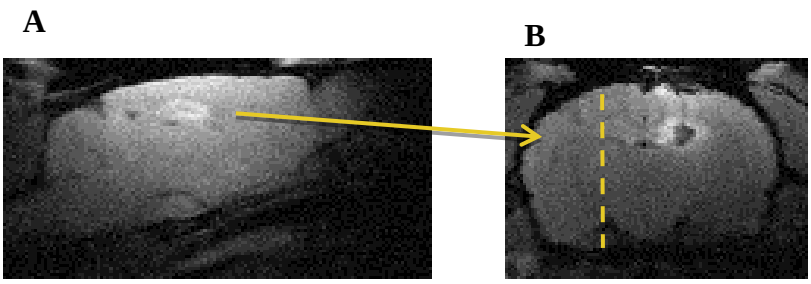

Figure 2.6: A: Sagittal image of the enhancement in the hippocampus contralateral to the cannula indicating transport across the midline as shown in B: coronal image of 28 day Mn subject.

2.4.3 Rat 150- Lesion

After 10 days post-surgery, a hypointense region began to appear in the brain of the 28-day Mn rat. Figure 2.7 shows the progression of this region over time. This black region did not appear in the 28 day control, 7 day Mn or the 7 day control. . Figure 2.7 indicates that this damage occurs after about 13 days. At approximately 13 days, the volume of Mn delivered was roughly 90 µl.

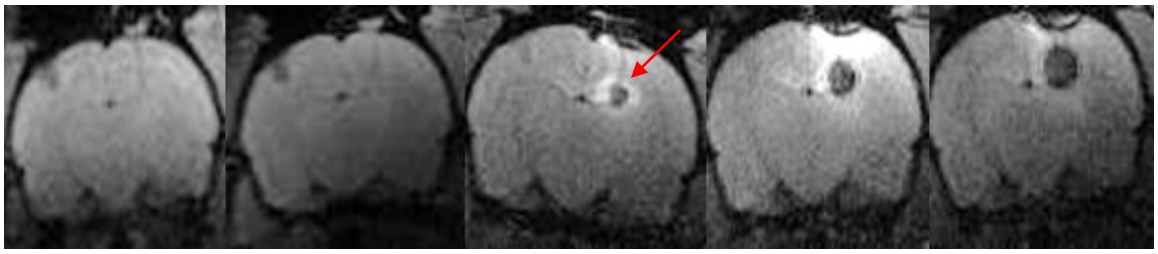

Figure 2.7: Coronal images of 28 day Mn showing progression of the lesion (red arrow indicates lesion). Images represent days 5,13,19,25 and 28 post-surgery. Tissue damage on the first two images in the top left hemisphere is due to the screws implanted during surgery.

2.4.4 Histology

Using cresyl violet histology it was confirmed that the black mass observed in the 28-day Mn rat was a lesion (Figure 2.8C). Figure 2.8 shows the corresponding brain slices to the MRI images of rats 150 and 152. In cresyl violet stained histological sections, a region of cell loss within the Mn injection site with a length of approximately 0.67 mm was observed (Figure 2.8D). This result indicates that localized cell death occurred near the tip of the cannula. The control experiments did not show significant cell damage confirming that the cause was due to the Mn cytotoxicity in the solution.

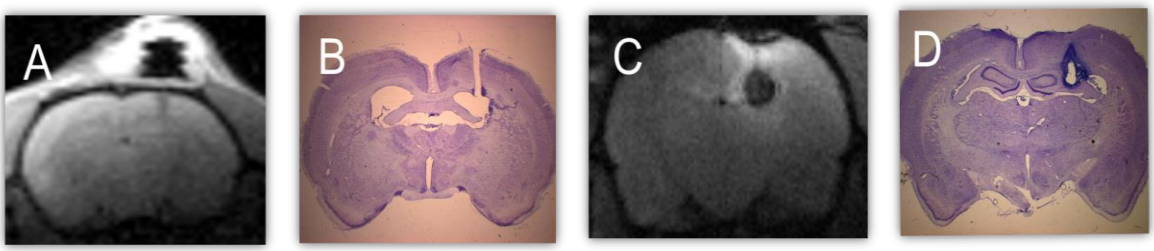

Figure 2.8: Histological slices (cresyl violet) corresponding to MRI images indicating the extent of cell damage. A: 28-day control MRI B: histological slice 28-day control C: 28-day Mn D: histological slice 28-Day Mn.

2.4.5 Behavioural Observations

2.4.5.1 Skilled Reaching Task

Observations in the single pellet reaching task demonstrated that the Mn had no effect on the fine motor skills (using student's t-test, P=0.68 for 28-day and P=0.5 for 7-day rat) (Figure 2.9). Qualitative analyses also showed that there was no change in fine motor skills after Mn infusion.

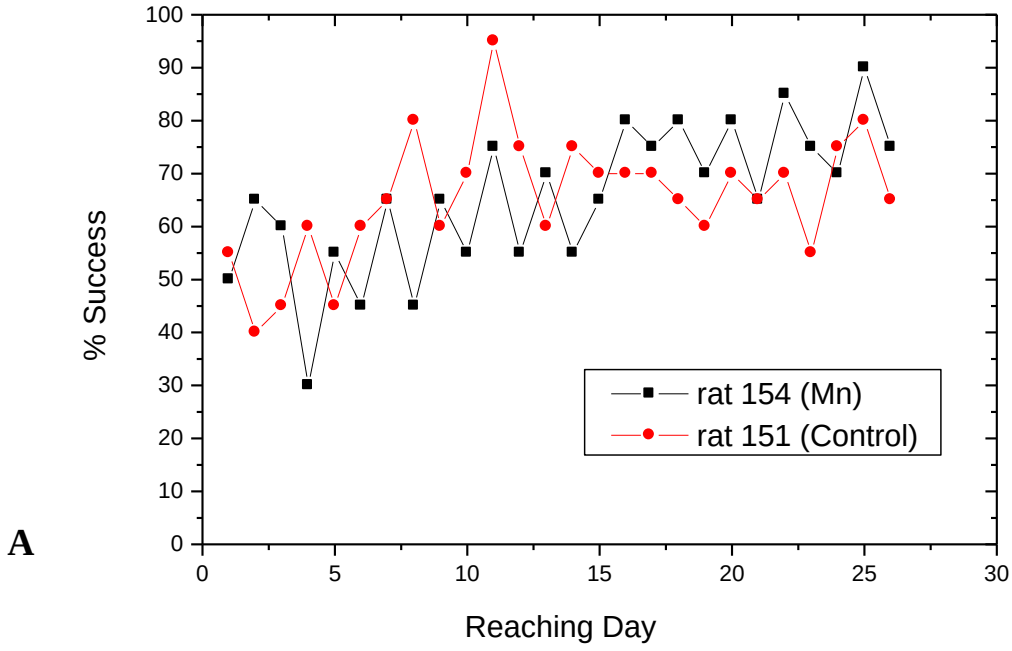

A

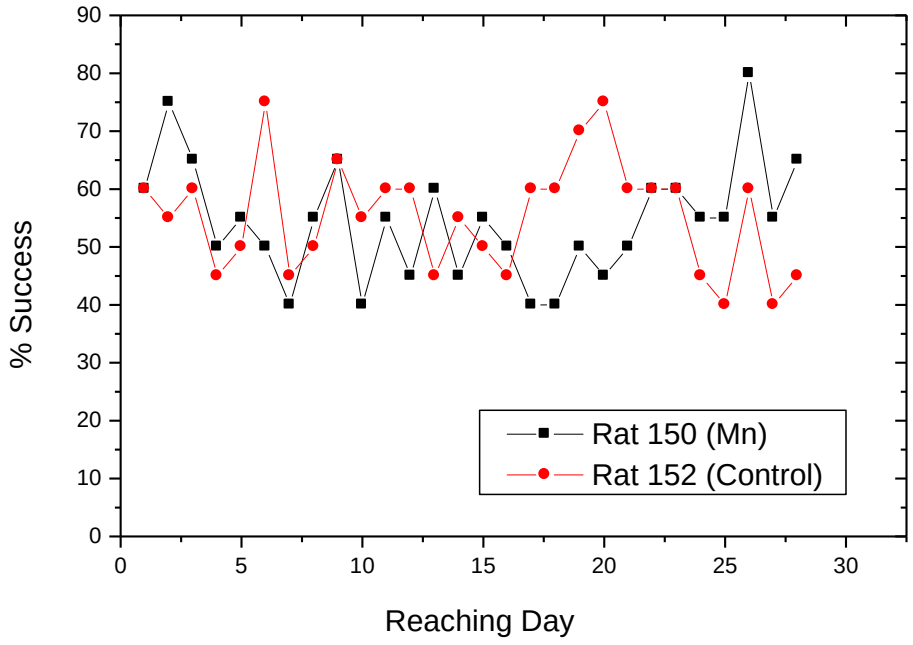

B

Figure 2.9: Percent success (measured as: # of successful reaches/# of total reaches) over reaching days of the A: 7 day pump rats and the B: 28 day pump rats. P=0.68 for 28-day and P=0.5 for 7-day rat. Rats maintained reaching success over the course of Mn treatment.

2.4.5.2. Body weight

Figure 2.10 shows the average weight of rats pre- and post-surgery. There were no significant changes in the body weight during the course of the study.

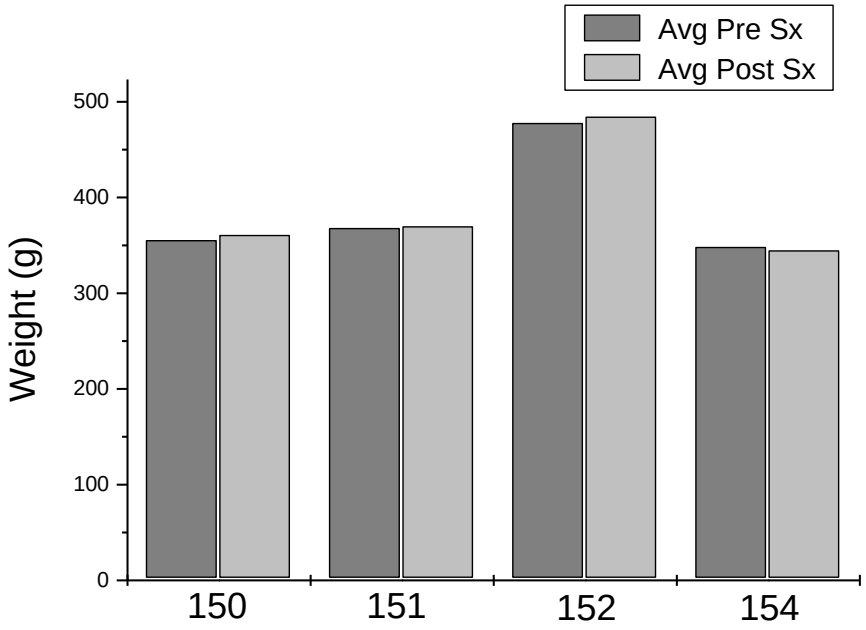

Figure 2.10: Average weight of rats pre- and post-surgery.

2.5 Discussion

2.5.1 T1 Relaxation Time Due to Mn Infusion

The findings of the present study illustrate the successful application of an intracerebroventricular cannula and osmotic pump system to administer Mn to the rat brain. To my knowledge, this is the first time an osmotic pump was used to deliver Mn to the lateral ventricle. Results indicate that a concentration of 0.85 mM delivered over 7 days, and a concentration of 100 mM delivered over 28 days are both sufficient to

produce MRI-detectable Mn levels. A higher T1 rate in Mn-treated rats is expected because the rate of T1 relaxation is directly proportional to the Mn concentration (Silva et al., 2004). Hence, the higher the Mn concentration, the higher the T1 rate.

The present findings also indicate that the relaxation rate change due to the delivery of Mn plateaus after approximately 20 days when using the 28 day pump. Unfortunately, there are no studies which have used a slow release technique (28 days) to compare these results to. However, it could be postulated that these findings could be due to the cell death caused by relatively high Mn concentration. This may have decreased or restricted Mn flow to the surrounding brain tissue as the transport mechanism may have been blocked by the dead cells. This result is similar to a study that administered 120 mM Mn focally into the medial thalamus (Yang et al., 2011). They also caused a lesion due to high concentrations of Mn and found that the subsequent signal enhancement was focal with a small deposition of Mn to other areas. Another explanation for the restricted flow of Mn to the site of injection could be due to the accumulation of Mn given the high density of astroglia and their reaction to the tissue damage (Kawai et al., 2010). Astroglia act as metal depots (Tiffany-Castiglioni and Qian, 2001) and one of their roles includes the repair and scarring of brain and spinal cord tissue following traumatic injuries. Thus, the presence of tissue damage could attract Mn primarily to this area.

Mn delivery from the 7-day pump peaked on the last day of delivery contrary to the 28-day pump which peaked on day 14 (mid-way). This is analogous to bolus systemic injections that use higher concentrations or slow release administrations with osmotic pumps (Eschenko et al., 2010a). This indicates that using a direct injection to the lateral

ventricle could be used alternately to systemic injections. Like systemic injections, enhancement is prominent in regions such as the hippocampus (Aoki et al., 2004b).

2.5.2 Enhancement in the Hippocampus

In the present study, Mn was detectable in the brain and was prominently accumulated in the hippocampal region. This result is analogous to other studies that showed a movement of Mn from the CSF to brain tissue (Liu et al., 2004, Jeong et al., 2012). Moreover, these results validate the theory that signal enhancement primarily in the hippocampus is caused by Mn absorption from the ventricles (Aoki et al., 2004c, Bock et al., 2008). Also, as described in Chapter 1, it has also been shown that the distribution of manganese may reflect the density and or activity of astrocytes (Henriksson and Tjalve, 2000), neurons (Pautler et al., 1998), or mitochondria (Akai et al., 1990, Gavin et al., 1990). It may be a combination of the location and composition of the hippocampus which causes it to have high signal intensity due to Mn.

This noticeable detectability in the hippocampus can allow researchers to take advantage of this technique for studies which focus on the anatomy or activity of the hippocampus (Lui et al., 2011, Palacios et al., 2011). From the results of this study, it is obvious that the higher concentration of Mn shows a larger change in hippocampal enhancement whereas the lower concentration has a small change. This suggests that in order to achieve large changes in hippocampal enhancement, concentrations higher than 0.85 mM are necessary. Consequently, increasing the concentration may cause hindrances when it comes to studies of behavior. One study has already shown that that 200 mM/kg Mn produces hippocampal MR signal enhancement without disrupting

hippocampus-dependent behavior. They used a rapid place learning task indicating that studies could apply behavioural testing while using MEMRI (Jackson et al., 2011). The present study also reveals insights into the behavioural significances of Mn toxicity.

2.5.3 Behaviour

Mn treatment typically results in decreased motor activity or disturbances in motor coordination as well as Mn-induced hyperactivity (Eriksson et al., 1987, Calabresi et al., 2001). However, this study shows that in all cases, the behaviour was not significantly affected by the infusion. This could be explained by the ability of a focal intracerebral injection to bypass the systemic system, which reduces the risk of complications. Furthermore, a study showed that the slow administration of Mn over a long period of time reduced behavioural deficits seen when using bolus injections (Eschenko et al., 2010a). The combination of these two factors; direct injection and slow infusion, leads to an appropriate method of reducing Mn-associated neurotoxicity (for 0.85 mM) and spared behavioural function.

Also, the present findings show an absence of significant changes in body weight during the time-course of Mn administration. This could indicate that the focal injections, because they bypass the systemic system, are less stressful to the rat's health as they are able to maintain body weight.

2.5.4 Histology and Lesion

The evaluation of cresyl violet-stained sections revealed that Mn can be delivered without cell damage at a concentration of 0.85 mM and at a rate of 1 µl/hr over 7 days.

Inspection of the histological data, however, indicated that administering Mn at a concentration of 100 mM with an infusion rate of 0.25 µL/hr over 28 days caused cell damage. Findings indicate that a concentration of or exceeding 100 mM was not suitable for intracerebral injections. A slow release mechanism using an osmotic pump still did not alleviate the neurotoxic effects of 100 mM Mn. These data contradict a recent study suggesting that under conditions of continuous infusion, Mn was continuously transported away from the infusion site by neurons and detoxified by glial cells, which prevented the tissue concentration from reaching a toxic threshold (Canals et al., 2008). This might only be the case when the concentration is low enough to prevent the formation of reactive glial cells, which attract Mn to areas of brain distress instead of being removed from the infusion site.

Another interesting finding was based on a comparison of lesion sites between studies. The data is comparable to images obtained by Seo et al. (2011). Although these authors showed similar MRI results, their "lesion" was attributed to a different cause than neurotoxicity. In their study they administered a concentration of 2 mM Mn-bicine at 50 µl/ hr and stated that the "dark mass" which appeared was simply an artifact in the left ventricle of the image (Seo et al., 2011). They attributed the hypointense region of interest to a high concentration of Mn or high intensity due to Mn. This is a possibility as these authors used a microinjection of a smaller concentration. However, without histological evaluation, it is impossible to confirm the mass as an image artifact and not a lesion. This result enforces the importance of histology when developing MEMRI applications.

2.6 Conclusion

Many studies have explored the route of Mn injections, toxicity of injection dose, sensitivity to anatomical structure analysis and changes in signal intensity over a time course after injection. However, there is no consistent method for the administration of Mn, even when comparing between studies with a similar method of administration. The efficacy of MEMRI could benefit from the development of consistent methodologies for each type of administration and purpose. However, studies of various models are needed to better analyze the different injection routes of Mn and the optimal doses before a consistent procedure is created.

In this study, a method for the application of Mn to the lateral ventricle was used. It was shown that a low dose delivery of Mn at 0.85 mM, using a 7-day osmotic pump, showed detectable changes in MRI without causing adverse toxic effects. The importance of behavioural testing and histology was demonstrated by the findings that the application of a high Mn concentration at 100 mM over 28 days causes severe cell damage at the tip of the cannula.

Future Studies

This project represented a pilot investigation of a high and low dose application of Mn for MEMRI. Observations suggest that a comparison of medium-dose Mn concentrations is necessary to evaluate the range of Mn-induced effects on toxicity and imaging parameters. Histology and behavioural tests should be applied to assist in determining the boundaries of the applications of MEMRI. Further work is needed in these areas and technical issues must be considered. An experiment using 2 mM Mn

delivered over 7 days is in the planning stages. Also a solenoid surface coil which has an open area in the center to prevent contact with the cannula is being fabricated. With these improvements, MEMRI will prove to be an extremely useful imaging tool for structural and functional analysis in neuroscientific studies.

2.7 References

Akai F, Maeda M, Suzuki K, Inagaki S, Takagi H, Taniguchi N (1990) Immunocytochemical localization of manganese superoxide dismutase (Mn-SOD) in the hippocampus of the rat. Neurosci Lett 115:19-23.

Aoki I, Naruse S, Tanaka C (2004a) Manganese-enhanced magnetic resonance imaging (MEMRI) of brain activity and applications to early detection of brain ischemia. Nmr in Biomedicine 17:569-580.

Aoki I, Wu YJ, Silva AC, Lynch RM, Koretsky AP (2004b) In vivo detection of neuroarchitecture in the rodent brain using manganese-enhanced MRI. Neuroimage 22:1046-1059.

Aoki I, Wu YJL, Silva AC, Lynch RM, Koretsky AP (2004c) In vivo detection of neuroarchitecture in the rodent brain using manganese-enhanced MRI. Neuroimage 22:1046-1059.

Bitar R, Leung G, Perng R, Tadros S, Moody AR, Sarrazin J, McGregor C, Christakis M, Symons S, Nelson A, Roberts TP (2006) MR pulse sequences: what every radiologist wants to know but is afraid to ask. Radiographics : a review publication of the Radiological Society of North America, Inc 26:513-537.

Bloch F, Hansen WW, Packard M (1946) The Nuclear Induction Experiment. Phys Rev 70:474-485.

Bock NA, Paiva FF, Nascimento GC, Newman JD, Silva AC (2008) Cerebrospinal fluid to brain transport of manganese in a non-human primate revealed by MRI. Brain research 1198:160-170.

Bouilleret V, Cardamone L, Liu C, Koe AS, Fang K, Williams JP, Myers DE, O'Brien TJ, Jones NC (2011) Confounding Neurodegenerative Effects of Manganese for In Vivo MR Imaging in Rat Models of Brain Insults. Journal of Magnetic Resonance Imaging 34:774-784.

Calabresi P, Ammassari-Teule M, Gubellini P, Sancesario G, Morello M, Centonze D, Marfia GA, Saulle E, Passino E, Picconi B, Bernardi G (2001) A synaptic mechanism underlying the behavioral abnormalities induced by manganese intoxication. Neurobiology of disease 8:419-432.

Canals S, Beyerlein M, Keller AL, Murayama Y, Logothetis NK (2008) Magnetic resonance imaging of cortical connectivity in vivo. Neuroimage 40:458-472.

Chen W, Tenney J, Kulkarni P, King JA (2007) Imaging unconditioned fear response with manganese-enhanced MRI (MEMRI). Neuroimage 37:221-229.

Chuang K-H, Koretsky AP, Sotak CH (2009a) Temporal Changes in the T1 and T2 Relaxation Rates (R1 and R2) in the Rat Brain Are Consistent With the Tissue-Clearance Rates of Elemental Manganese. Magnetic Resonance in Medicine 61:5.

Chuang KH, Koretsky AP, Sotak CH (2009b) Temporal changes in the T1 and T2 relaxation rates (DeltaR1 and DeltaR2) in the rat brain are consistent with the tissue-clearance rates of elemental manganese. Magnetic resonance in medicine : official journal of the Society of Magnetic Resonance in Medicine / Society of Magnetic Resonance in Medicine 61:1528-1532.

Cross DJ, Minoshima S, Anzai Y, Flexman JA, Keogh BP, Kim YM, Maravilla KR (2004) Statistical mapping of functional olfactory connections of the rat brain in vivo. Neuroimage 23:1326-1335.

de Sousa PL, de Souza SL, Silva AC, de Souza RE, de Castro RM (2007) Manganese-enhanced magnetic resonance imaging (MEMRI) of rat brain after systemic administration of MnCl2: changes in T-1 relaxation times during postnatal development. Journal of Magnetic Resonance Imaging 25:32-38.

Eriksson H, Lenngren S, Heilbronn E (1987) Effect of long-term administration of manganese on biogenic amine levels in discrete striatal regions of rat brain. Archives of toxicology 59:426-431.

Eschenko O, Canals S, Simanova I, Beyerlein M, Murayama Y, Logothetis NK (2010a) Mapping of functional brain activity in freely behaving rats during voluntary running using manganese-enhanced MRI: Implication for longitudinal studies. Neuroimage 49:2544-2555.

Eschenko O, Canals S, Simanova I, Logothetis NK (2010b) Behavioral, electrophysiological and histopathological consequences of systemic manganese administration in MEMRI. Magnetic Resonance Imaging 28:1165-1174.

Gavin CE, Gunter KK, Gunter TE (1990) Manganese and calcium efflux kinetics in brain mitochondria. Relevance to manganese toxicity. The Biochemical journal 266:329-334.

Hahn EL (1950) Spin Echoes. Phys Rev 80:580-594.

Henriksson J, Tjalve H (2000) Manganese taken up into the CNS via the olfactory pathway in rats affects astrocytes. Toxicological sciences : an official journal of the Society of Toxicology 55:392-398.

Huettel SA, Song, Allen W., Mccarthy Gregory (2009) Functional Magnetic Resonance Imaging. 23 Plumtree road, Sunderland, M.A. USA: Sinauer associates, Inc.

Inui-Yamamoto C, Yoshioka Y, Inui T, Sasaki KS, Ooi Y, Ueda K, Seiyama A, Ohzawa I (2010) The brain mapping of the retreival of conditioned taste aversion memory using manganese-enhanced magnetic resonance imaging in rats Neuroscience 167:199-204.

Jackson SJ, Hussey R, Jansen MA, Merrifield GD, Marshall I, MacLullich A, Yau JL, Bast T (2011) Manganese-enhanced magnetic resonance imaging (MEMRI) of rat brain after systemic administration of MnCl(2): hippocampal signal enhancement without disruption of hippocampus-dependent behavior. Behav Brain Res 216:293-300.

Jeong KY, Lee C, Cho JH, Kang JH, Na HS (2012) New Method of Manganese-Enhanced Magnetic Resonance Imaging (MEMRI) for Rat Brain Research. Experimental animals / Japanese Association for Laboratory Animal Science 61:157-164.

Kang YS, Gore JC (1984) Studies of tissue NMR relaxation enhancement by manganese. Dose and time dependences. Investigative radiology 19:399-407.

Kawai Y, Aoki I, Umeda M, Higuchi T, Kershaw J, Higuchi M, Silva AC, Tanaka C (2010) In vivo visualization of reactive gliosis using manganese-enhanced magnetic resonance imaging. Neuroimage 49:3122-3131.

Keevil SF (2001) Magnetic Resonance imaging in medicine. Physics education 36:9.

Kuo YT, Herlihy AH, So PW, Bhakoo KK, Bell JD (2005) In vivo measurements of T1 relaxation times in mouse brain associated with different modes of systemic administration of manganese chloride. Journal of Magnetic Resonance Imaging 21:334-339.

Lin YJ, Koretsky AP (1997) Manganese ion enhances T-1-weighted MRI during brain activation: An approach to direct imaging of brain function. Magnetic Resonance in Medicine 38:378-388.

Liu CH, D'Arceuil HE, de Crespigny AJ (2004) Direct CSF injection of MnCl2 for dynamic manganese-enhanced MRI. Magnetic Resonance in Medicine 51:978-987.

Lui CC, Wang JY, Tain YL, Chen YC, Chang KA, Lai MC, Huang LT (2011) Prenatal stress in rat causes long-term spatial memory deficit and hippocampus MRI abnormality: Differential effects of postweaning enriched environment. Neurochemistry International 58:434-441.

Metz GAS, Whishaw IQ (2000) Skilled reaching an action pattern: stability in rat (Rattus norvegicus) grasping movements as a function of changing food pellet size. Behavioural Brain Research 116:111-122.

Murayama Y, Weber B, Saleem KS, Augath M, Logothetis NK (2006) Tracing neural circuits in vivo with Mn-enhanced MRI. Magn Reson Imaging 24:349-358.

Palacios RDY, Campo A, Henningsen K, Verhoye M, Poot D, Dijkstra J, Van Audekerke J, Benveniste H, Sijbers J, Wiborg O, Van der Linden A (2011) Magnetic Resonance Imaging and Spectroscopy Reveal Differential Hippocampal Changes in Anhedonic and Resilient Subtypes of the Chronic Mild Stress Rat Model. Biological Psychiatry 70:449-457.

Pautler RG (2006) Biological applications of manganese-enhanced magnetic resonance imaging In: Magnetic Resonance Imaging: Methods and biological applications vol. 124 (Pottumarthi, P. V., ed), p 28 Totowa, New Jersey: Humana Press.

Pautler RG, Silva AC, Koretsky AP (1998) In vivo neuronal tract tracing using manganese-enhanced magnetic resonance imaging. Magnetic Resonance in Medicine 40:740-748.

Purcell EM, Torrey HC, Pound RV (1946) Resonance Absorption by Nuclear Magnetic Moments in a Solid. Phys Rev 69:37-38.

Roth JA (2006) Homeostatic and toxic mechanisms regulating manganese uptake, retention, and elimination. Biological research 39:45-57.

Sandvig A, Sandvig I, Berry M, Olsen O, Pedersen TB, Brekken C, Thuen M (2011) Axonal Tracing of the Normal and Regenerating Visual Pathway of Mouse, Rat, Frog, and Fish Using Manganese-Enhanced MRI (MEMRI). Journal of Magnetic Resonance Imaging 34:670-675.

Seo Y, Satoh K, Watanabe K, Morita H, Takamata A, Ogino T, Murakami M (2011a) Mn-bicine: A Low Affinity Chelate for Manganese Ion Enhanced MRI. Magnetic Resonance in Medicine 65:1005-1012.

Seo Y, Takamata A, Ogino T, Morita H, Murakami M (2011b) Lateral diffusion of manganese in the rat brain determined by T(1) relaxation time measured by (1)H MRI. Journal of Physiological Sciences 61:259-266.

Sepulveda MR, Dresselaers T, Vangheluwe P, Everaerts W, Himmelreich U, Mata AM, Wuytack F (2012) Evaluation of manganese uptake and toxicity in mouse brain

during continuous MnCl(2) administration using osmotic pumps. Contrast media & molecular imaging 7:426-434.
Silva AC, Bock NA (2008) Manganese-enhanced MRI: An exceptional tool in translational neuroimaging. Schizophrenia Bulletin 34:595-604.
Silva AC, Lee JH, Aoki I, Koretsky AP (2004) Manganese-enhanced magnetic resonance imaging (MEMRI): methodological and practical considerations. NMR Biomed 17:532-543.
Tambalo S, Daducci A, Fiorini S, Boschi F, Mariani M, Marinone M, Sbarbati A, Marzola P (2009) Experimental Protocol for Activation-Induced Manganese-Enhanced MRI (AIM-MRI) Based on Quantitative Determination of Mn Content in Rat Brain by Fast T-1 Mapping. Magnetic Resonance in Medicine 62:1080-1084.
Theeuwes F, Yum SI (1976) Principles of the design and operation of generic osmotic pumps for the delivery of semisolid or liquid drug formulations. Annals of biomedical engineering 4:343-353.
Tiffany-Castiglioni E, Qian YC (2001) Astroglia as metal depots: Molecular mechanisms for metal accumulation, storage and release. Neurotoxicology 22:577-592.
Van der Linden A, Van Meir V, Boumans T, Poirier C, Balthazart J (2009) MRI in small brains displaying extensive plasticity. Trends in Neurosciences 32:257-266.
van der Zijden JP, Bouts M, Roeling TAP, Bleys R, van der Toorn A, Dijkhuizen RM (2008) Manganese-enhanced MRI of brain plasticity in relation to functional recovery after experimental stroke. Journal of Cerebral Blood Flow and Metabolism 28:832-840.
Watanabe T, Michaelis T, Frahm J (2001) Mapping of retinal projections in the living rat using high-resolution 3D gradient-echo MRI with Mn2+-induced contrast. Magnetic Resonance in Medicine 46:424-429.
Weng JC, Chen JH, Yang PF, Tseng WYI (2007) Functional mapping of rat barrel activation following whisker stimulation using activity-induced manganese-dependent contrast. Neuroimage 36:1179-1188.
Yang PF, Chen DY, Hu JW, Chen JH, Yen CT (2011) Functional tracing of medial nociceptive pathways using activity-dependent manganese-enhanced MRI. Pain 152:194-203.
Yu X, Wadghiri YZ, Sanes DH, Turnbull DH (2005) In vivo auditory brain mapping in mice with Mn-enhanced MRI. Nature neuroscience 8:961-968.

CHAPTER 3

Experiment 2: Application of MEMRI- F3 Generation Stress and MEMRI

3.1 Abstract

Prenatal stress has been proven to cause abnormal neuroanatomical, cognitive, behavioral and psychosocial outcomes in both humans and animals. The consequences of prenatal stress across generations of animals on these outcomes, however, have not been studied in detail. This study is the first to investigate the effect of transgenerational prenatal stress (TPS) on brain morphology in rats using MEMRI and histology. The results revealed that the experience of prenatal stress across three generations results in a 3% reduction in hippocampal volume and a 7 % reduction in whole brain volume. The percent volume of hippocampus in relation to whole brain volume, however, was not different in TPS rats versus control rats. This observation may indicate that the hippocampal volume changed as a function of whole brain volume. Additionally, this study investigated the use of a subcutaneous osmotic pump to deliver Mn for MEMRI. When Mn, is released slowly with the use of an osmotic pump, all rats showed a visible reduction in T1-relaxation in the hippocampus. These findings indicate that MEMRI represents a valid tool for the study of stress-induced changes in brain development.

3.2 Introduction

3.2.1 Prenatal and Transgenerational Stress

The perinatal period is a critical period for the development of the brain. As such, it is a very susceptible period for environmental and physiological factors, such as stress, to disturb homeostasis and development (Ruiz et al., 2005). The term stress is used to

describe any physical or psychological challenge that threatens, or has the potential to threaten the natural regulatory capacity of an organism (Koolhaas et al., 2011). Pregnancy and early development in the offspring represent a particularly vulnerable period to respond to environmental stressors. A recent cross sectional study found that 6% of pregnant women reported high levels of psychological stress, such as depression, panic disorder, or domestic violence, during their pregnancies, and 78% reported low to moderate levels (Woods et al., 2009).

The experience of stress by the pregnant mother activates the hypothalamic-pituitary-adrenal (HPA) axis to initiate the release of stress hormones, such as cortisol in humans or corticosterone in rats, which may enter the fetal circulation (Migeon et al., 1956, Takahashi et al., 1997, Williams et al., 1999). Thus, chronic stress may cause prolonged elevation in plasma cortisol in both the maternal and fetal circulation (Takahashi et al., 1998). Prenatally stressed offspring have been shown to exhibit heightened sensitivity to stress-induced HPA hormone secretion (Fride et al., 1986, Henry et al., 1994, Takahashi et al., 1988).

Studies demonstrated that a variety of different stress models in mice, rats and primates causes anatomical differences in brain regions such as the hippocampus as well as the prefrontal cortex (Palacios et al., 2011, Golub et al., 2011). More specifically, prenatal stress can cause negative effects on the hippocampal formation of offspring. These effects include inhibition of neurogenesis, reduction in hippocampal volume and resulting behavioural deficits in spatial memory (Zhu et al, 2004, Lemaire et al., 2000, Lucassen et al., 2009, Lui et al., 2011, Coe et al., 2003).

The hippocampal pyramidal neurons contain a high concentration of glucocorticoid receptors that are sensitive either to hypercortisolemia caused by severe stress or to exposure to exogenous glucocorticoids (McEwen, 2000). Work in an animal model showed that when exposed to high and/or long-term doses of corticosteroids or intensive stress, individuals suffered from structural and behavioural changes and often hippocampal neuronal death (Zach et al., 2010, Crews et al., 2012).

Given that most previous conclusions from animal studies are based on *ex-vivo* findings, this study aimed to assess consequences of TPS on the rat brain using MEMRI and comparisons to histology.

3.2.2 Application of MEMRI

3.2.2.1 Structure

Recently, the first MRI study on prenatal stress effects in animals was conducted, which revealed gross hippocampus pathology in prenatally stressed adult rats (Lui et al., 2011). Prior to this study, animal structural MRI has been used to show that chronic stress (chronic restraint, 6 hrs per day for 21 days) can reduce the overall size of the hippocampus (Lee et al., 2009). MRI was also able to report an approximate 3% decrease in hippocampal volume following chronic stress (Lee et al., 2009).

MEMRI is particularly suitable for longitudinal studies in rodent models of disorders in which hippocampal dysfunction has been implicated (Jackson et al., 2011). As shown in the previous chapter, Mn-induced signal enhancement is highly heterogenous across the brain, with some structures, including the hippocampus, showing particularly pronounced enhancement (Chapter 2). Recently, a study used MEMRI to

assess long-term consequences of post-traumatic stress disorder of hippocampal volume in mice (Golub et al., 2011). Using MEMRI, the authors were able to report a reduction in hippocampal size.

3.2.2.2 Uptake time

The technique of MEMRI is a unique tool to show not only vivid structural abnormalities, but also brain activation changes (due to uptake through Ca^{2+} channels) or uptake time of Mn (rate at which Mn is transported through the brain) in association with the metabolic response to stress (Cortez et al., 2008). Studies have used MEMRI to demonstrate that manipulations in mice significantly reduce signal intensity in multiple brain areas of fasted compared to *ad libitum* fed mice (Hankir et al., 2011, Kuo et al., 2005, Parkinson et al., 2009 and Chaudhri et al., 2006). Stress has been proven to have an effect on metabolism in human and animal studies. Therefore the uptake time of Mn between stressed and control groups will be investigated. Many, but not all, stressful events are accompanied by global increases in cerebral blood flow and/or energy metabolism (Byran et al., 1990). It may be possible to detect these changes with MEMRI, which represented the main aim of this experiment.

3.2.3 Objectives

For this study, great-grand-offspring (F3) generation stressed adult Long-Evans rats were compared to non-stressed rats using MEMRI with the delivery of $MnCl_2$ using a subcutaneously implanted osmotic pump. The hypothesis was that the stress effect from

the parental generations will be transferred to the F3 filial generation (Zucchi et al., 2012).

For this study, the aims were to:

1) Study changes in structure (whole brain and hippocampal),
2) Explore differences in uptake time (of $MnCl_2$) and,
3) Investigate differences in contrast (higher vs lower T1 due to the amount of Mn present in a set region).

Based on the current literature, to my knowledge, there is no model of transgenerational stress that has documented changes in brain morphology using MEMRI or histology.

3.3 Materials and Methods

3.3.1 Transgenerationally Stressed Rats

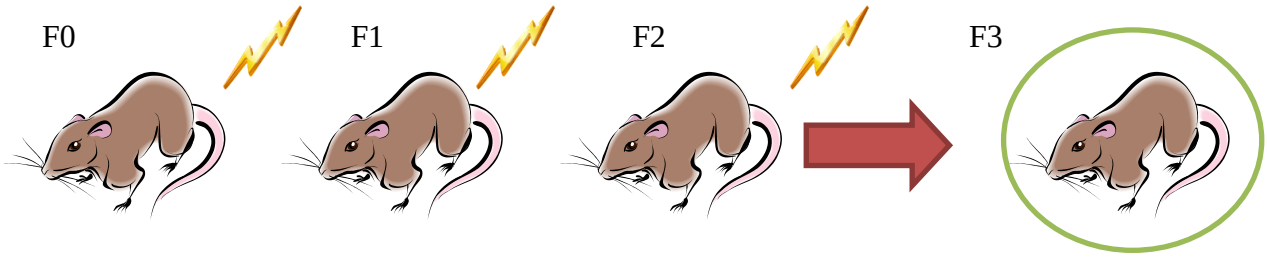

Figure 3.1: Schematic diagram representing gestational stress across generations and the offspring which were used in this study. Representation of Parental generation (F0), offspring (F1), grand-offspring (F2) and great-grand-offspring (F3) are shown here.

In order to obtain F3 transgenerational stressed rats, three generations of pregnant dams were stressed using restraint (Morley-Fletcher et al., 2003) and forced swimming (Porsolt et al., 1978) from gestational day 12 to 18. Stressors were given at semi-random alternations in the morning or afternoon. For restraint stress, animals were placed in restraint containers for 20 minutes daily. For swim stress, the animals were placed in a pool containing lukewarm water for 5 minutes.

3.3.2 Subjects and Housing

Twelve multigenerationally stressed F3 and six non-stressed F3 control female Long-Evans rats raised at the University of Lethbridge vivarium were used in this study. The animals were housed in pairs or triplets under a 12 hr light/day cycle with lights on at 7:30 AM. All subjects had access to food and water *ad libitum*. All procedures were performed in accordance with the guidelines of the Canadian Council for Animal Care at the University of Lethbridge.

3.3.3 Treatment

Eighteen Long-Evan female rats (90 days old and weighing 340 ± 35 g) were divided into two groups; multigenerationally stressed (n =12) and controls (n=6). Each rat was implanted with a 7-day ALZET osmotic pump with a concentration of 100 mM at an infusion rate of 1 µl/hr with a total volume of 200 µl. Based on the weight of the rat, the total dose delivered was approximately 7.14mg/kg. In all cases, the solution was pH-adjusted to 7.4 using NaOH and TRIS-HCL buffer.

3.3.4 Surgical Procedures

Rats were anesthetized according to the procedure outlined in Chapter 2. A small incision was made between the shoulder blades of the rat and a pocket under the skin was made using hemostats. The pump was inserted into the pocket and the incision closed with sutures. The contents of the pump were delivered into the local subcutaneous space. Absorption of the compound by local capillaries resulted in systemic administration. This lead to an indirect supply of $MnCl_2$ to the brain through the BCB. The osmotic pump allowed for continuous delivery of $MnCl_2$ over time.

3.3.5 MR Imaging

Imaging was performed using a 4.7 T 330 mm bore Oxford magnet (Oxford, UK) and a MR6000 (MR Solutions, UK) console. A 2-RF coil system consisting of a quadrature birdcage transmit coil (10cm in diameter, 10 cm in length, Morris Instruments, CAN), a homebuilt receive only butterfly coil (2 cm in diameter) and PIN diode switching was used. Control images were taken as baseline images prior to surgery. Following recovery, imaging took place every second day. The imaging protocol consisted of: a) Locator images (SE-TR/TE 700/13 ms, 0.2x0.2x1.5 mm), b) T1-weighted images (TE 15ms, TR=700 ms, 0.23x0.23x2 mm) c) T2-weighted images (TE=75 ms, TR=3000 ms, 0.23x0.23x2 mm) d) T1 measurements (TE=10 ms, TR=6000 ms, 0.47x0.47x2 mm) e) T2 measurements (TE=30,60,90 ms TR=2500 ms, 0.47x0.47x2 mm).

Signal intensity from regions of interest (ROI's) were extracted from the T1 images with Analyze 8.1 (BIR, USA) and T1 values were calculated using home written

software in IDL (ITT, USA). All images were co-registered (Figure 3.2A) and in some cases, the two sets of T2-weighted images were added together to obtain a higher signal-to-noise ratio (Figure 3.2B).

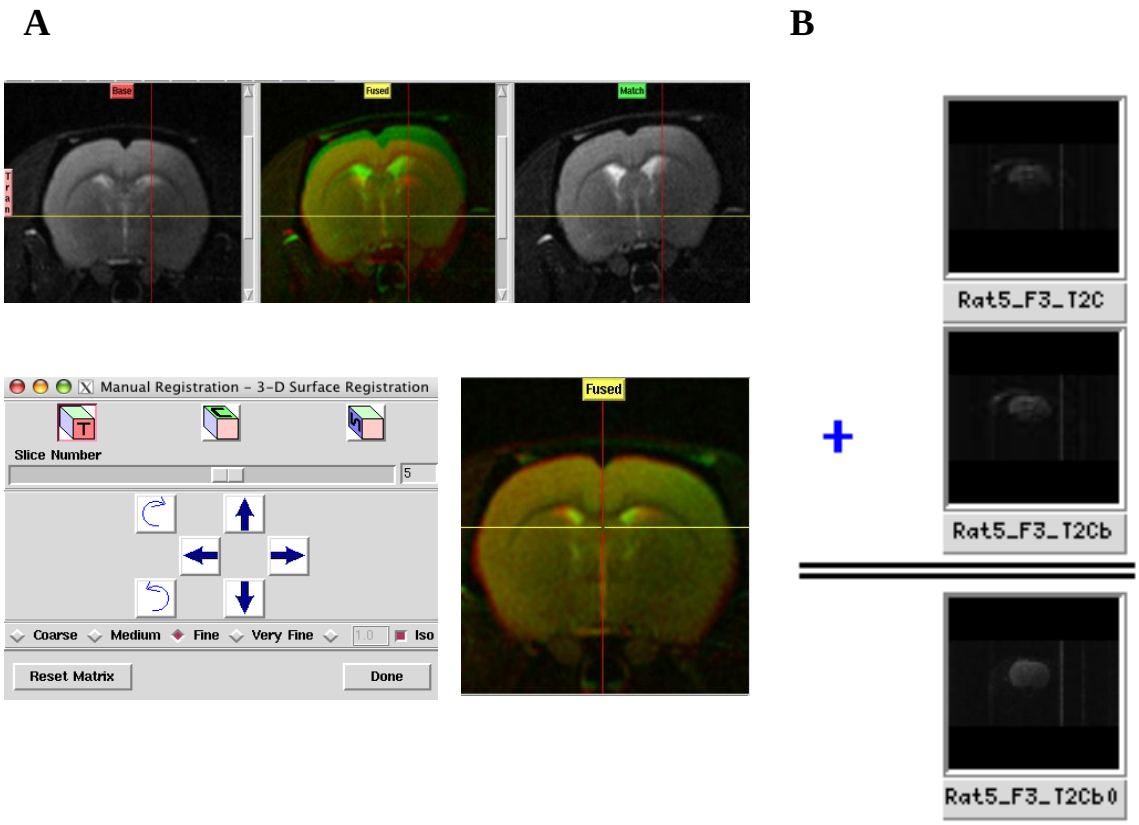

Figure 3.2: A) Analyze 8.1 co-registration showing a match image fused to a base T2-weighted coronal image. B) Image calculator, combining two T2-weighted images.

3.3.6 Histology

Rats were euthanized at the end of their pump duration (10 days post-surgery) with an injection of Euthansol (Merck, CAN). They were then perfused transcardially with PBS followed by a trancardial injection of 4% PFA both with a volume of 200 mL.

Brains were extracted and were then sectioned and sliced coronally using a microtome at a thickness of 40 µm. Twelve series were taken and stored in a 1X PBS with a 1:1000 concentration of sodium azide to prevent growth of bacteria or fungus. Every 3rd series was then mounted and stained with cresyl violet (for protocol, see Appendix B). The slides were captured using a Zeiss Axioimager M1 microscope (Zeiss, Germany) at 1X magnification (Figure 3.3).

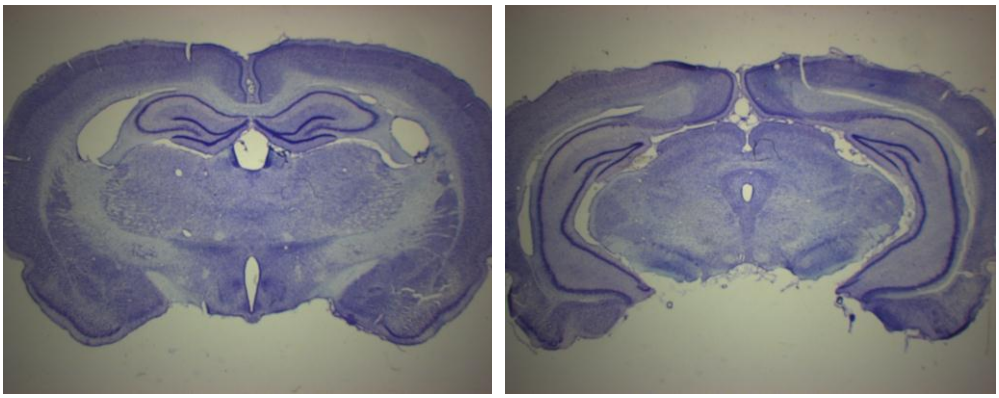

Figure 3.3: Examples of cresyl violet histology. Coronal sections taken through the hippocampus of are displayed here.

3.3.7 Volumetric Measures

3.3.7.1 MEMRI

A traced contour of the whole brain was manually drawn on each of the seven slices from T1 and T2-weighted images on the control and last day of Mn delivery, using Analyze 8.1 (BIR, USA). The hippocampal volume was manually traced and was calculated with 2 slices corresponding approximately -2.12 mm and -5.5 mm from bregma. Measurement boundaries were defined according to Wolf et al. (Wolf et al., 2002) and by referring to the rat atlas of the brain (Paxinos and Watson, 1998).

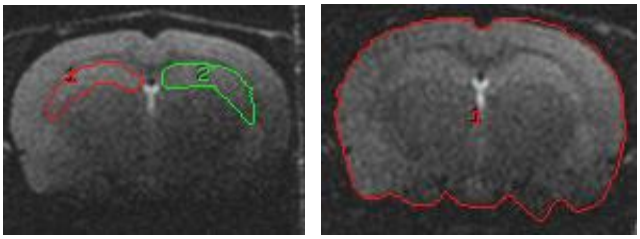

Figure 3.4: The whole brain ROI is shown to the right in red. The left (red) and right (green) hippocampal ROI's are shown to the left.

3.3.7.2 Histology

The volumetric measurements of the hippocampus were made on all but one structure within the hippocampal formation. Included were the subfields CA1-CA3 and the dentate gyrus of the hippocampus. Excluded was the entorhinal cortex (EC) because the precise boundary between the EC and the rest of the cortex was not clearly defined through the Nissl staining. Measurement boundaries were defined as reported previously (Verstynen et al., 2001).

The relevant hippocampal areas were determined according to the stereotaxic atlas of the rat brain (Paxinos and Watson, 1998) and measured using Image J analysis package (NIH, USA) for PC. The volume of each hippocampus was calculated as the sum of the product between the area on each slice and the inter-slice distance. In case a slice was missing or damaged the area was estimated by taking the average of the areas from the slices immediately posterior and anterior to the missing slice. Averaging was necessary for approximately 4-7 slices for each rat.

3.4 Results

3.4.1 Analysis of T1 Relaxation Rates

All statistical computations were performed using SPSS 13.0 software (IBM, USA). All graphs were created using Origin 5.0 lab freeware (Originlab, USA). Results show that Mn was transferred to the brain using the systemic application of the osmotic pump. Figure 3.5 shows that the concentration used was not sufficient to produce large changes in T1 relaxation times, however, they were significant (using student's t-test, n=18, p=0.007). Consequently, there was no significant difference (p=0.274) in uptake time between the stressed groups and the control group. Figure 3.6 shows the increase in hippocampal signal from control to day 8 of Mn administration.

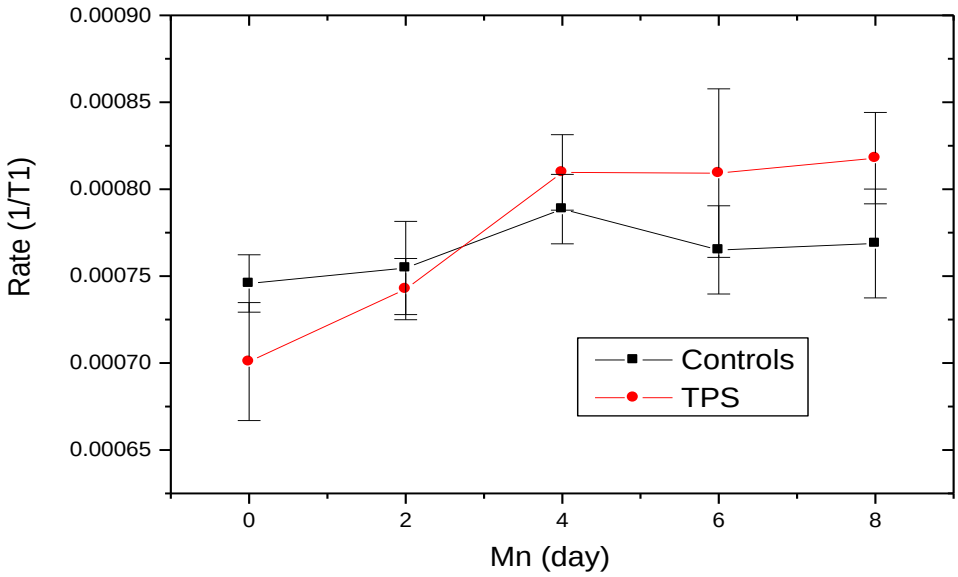

Figure 3.5: T1- rate (ms^{-1}) taken using the average whole brain ROI. Error bars represent the standard error of the mean (SEM). Control (n=6) TPS (n=12).

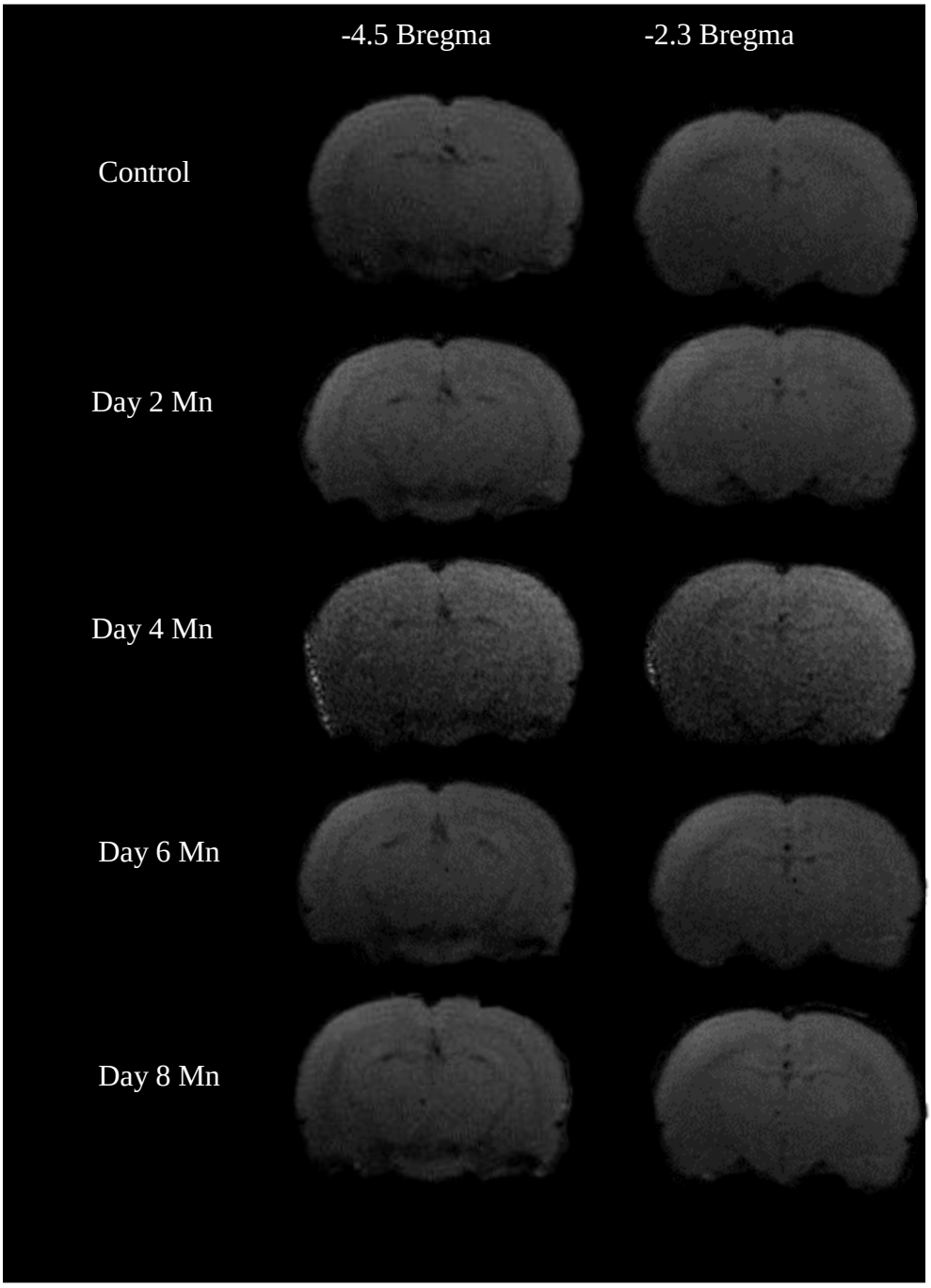

Figure 3.6: Coronal images of 2 slices corresponding to -2.3 and -4.5mm from bregma. Increasing in signal enhancement is shown as an increase in manganese concentration of days post-surgery.

3.4.2 Volumetric Analysis

3.4.2.1 MRI

From the whole brain ROI's drawn on the T1 and T2-weighted MRI images, the results as shown in Figure 3.7 were obtained. On average, stressed rats had whole brain volumes which were 7% smaller than controls (p=0.002). There was no significant change in volume between the control and last day of Mn delivery images.

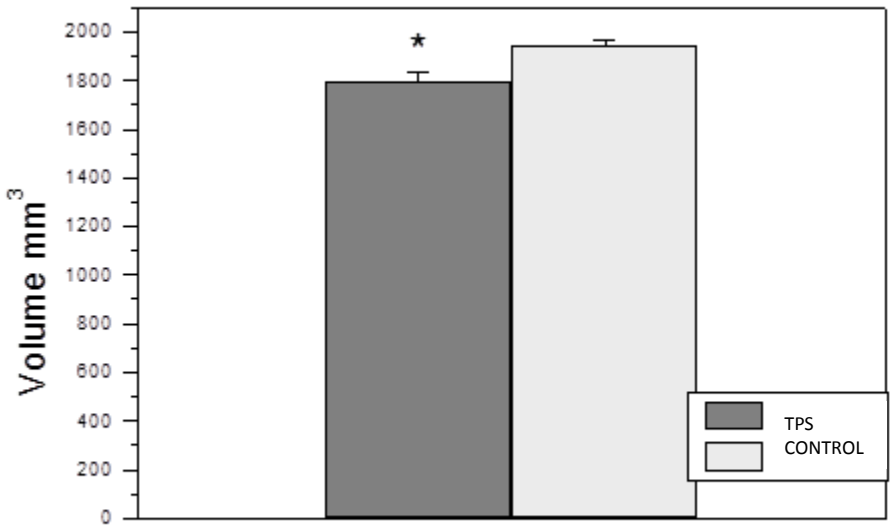

Figure 3.7: Volume (mm^3) of the whole brain MRI showing a reduction in TPS volume. Error bars represent the SEM. *p<0.05.

Animals in the TPS group showed a 15% reduction in hippocampal volume (Figure 3.7). These results were found to be significant (p<0.001). There was some difficulty drawing ROI's on the hippocampus of the T1 and T2-weighted images. In some cases T1 images were easier to trace ROIs and in other cases it was easier to trace on T2 images. Therefore an average of T1-weighted and T2-weighted ROI's were used.

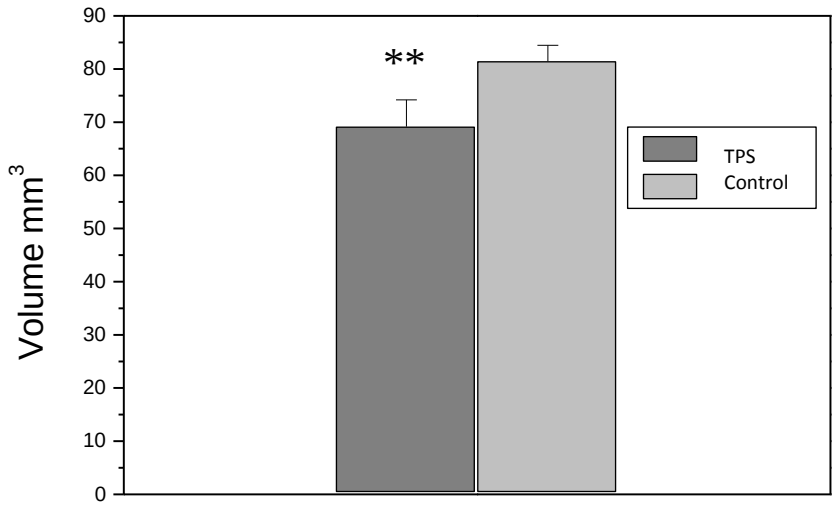

Figure 3.8: Volume (mm^3) of the hippocampus from MRI images showing a decrease in TPS volume. Error bars represent the SEM **p<0.001.

3.4.2.2 Histology

When comparing the average hippocampal volumes of TPS rats to control rats, there was a 3% reduction in volume. These values were found to be significant (p=0.009). However, hippocampal volumes relative to the whole brain volumes were found to be equally distributed between the TPS group and the control group (Figure 3.9). For percent difference, hippocampal ROI's from histological slices and whole brain MRI's were used. A correlation between a whole MRI slice and corresponding histology slice was made and found to be relatively similar (±0.9mm^2).

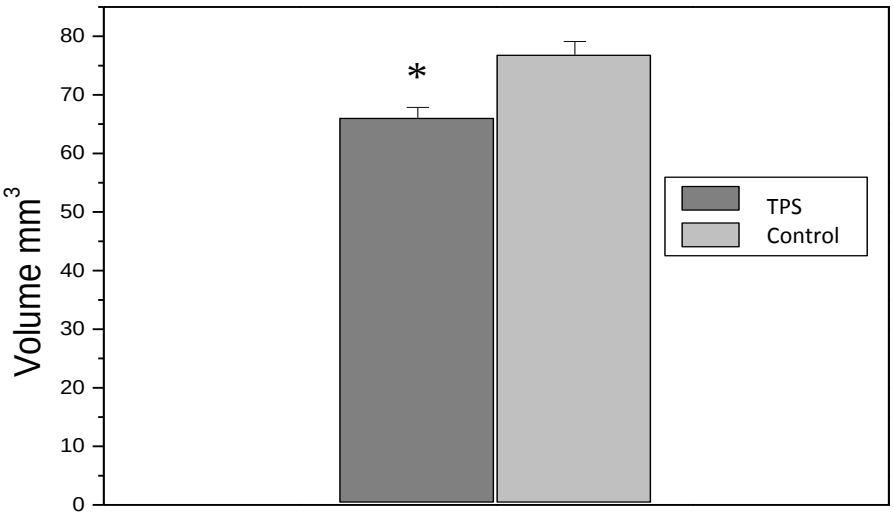

Figure 3.9: Volume (mm^3) of the hippocampus from Nissl stained slices. Error bars represent the SEM * $p<0.05$.

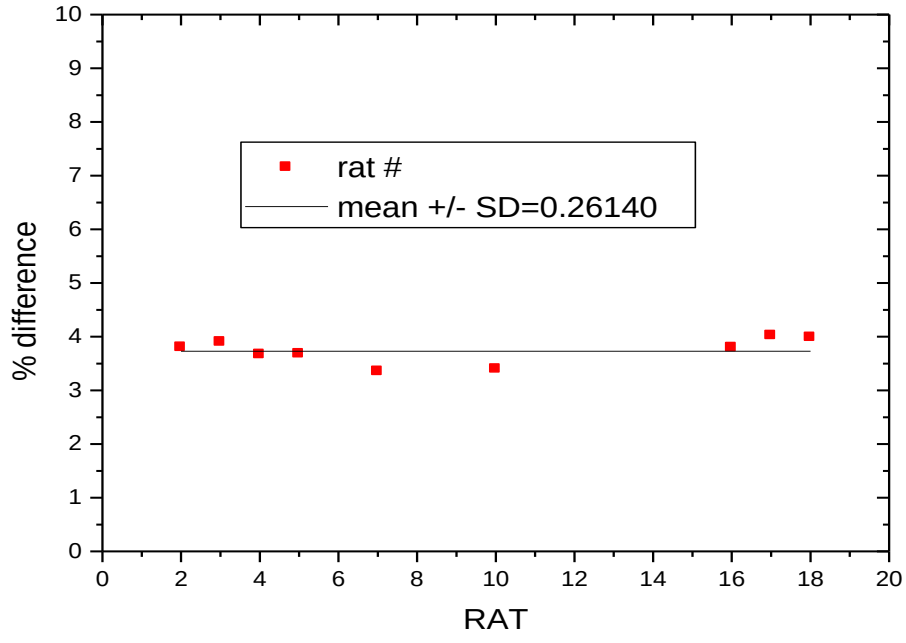

Figure 3.10: Relative change in hippocampal volume to whole brain volume. %change= (Hippocampal Volume/ Whole brain Volume) x 100

3.4.2.3 Weight Change

The change in body weight was calculated by subtracting the one-week average body weight prior to pump implantation. Weight loss within these rats was variable and there was no significance ($p>0.05$) between TPS and control groups. On average, rats lost around 8 ± 7g of body weight with the highest weight loss of being 20g.

3.5 Discussion

3.5.1 Relaxation Time due to Mn

In this study, F3 TPS rats were compared to non-stress control rats using MEMRI and histology. Investigated was brain structure (primarily changes in hippocampal volume) and differences in uptake time of Mn from F3 generation stressed rats compared to controls.

Results indicate that the concentration of Mn used was not high enough to detect changes in uptake time of Mn between TPS and control rats. Figure 3.6 shows an increasing trend in Mn concentration in both the TPS group and the control group. Comparing F3 TPS rats to control rats, the TPS rats have a higher Mn concentration than control rats, but these results were not significant. Further study is required to answer this question. Results could be clearer if a higher concentration of Mn was used. This could be achieved with a larger osmotic pump, to be discussed in chapter 4.

Nevertheless, with the concentration used, there was an increased enhancement in the hippocampus in the T1-weighted images. Both the T1 and T2-weighted images for ROI assessment of the whole brain and the hippocampal volumes were used. From the ROI's drawn, it was determined that the average whole brain volume of the TPS rats was

reduced by approximately 7% compared to control rats. Also, it was found that the hippocampal volume was decreased by approximately 15%. However, from the ROI's drawn on the histological slices, more precise measurements of hippocampal volume were obtained compared to those obtained from MRI. It was found that the TPS rat's hippocampus is on average 3% smaller than the control rat.

These results suggest three reasons why there was a difference in volumes obtained in MRI versus histology. The first is that from the resolution obtained, it was difficult to determine the hippocampal boundaries on MRI as the contrast to noise was low. Also, the resolution obtained with the control images (taken a month after assessment of the TPS rats) was of better quality due to internal or external variable noise beyond my control. Second, the SNR differed from day to day which caused inconsistencies in assessment. Lastly, it is easier to draw ROI's on the stained slices as the spatial resolution is higher. Histology has proven to be a more reliable method for determining volumes in this study. This is because of the higher resolution obtained as well as the number of slices which were used to calculate volume with histology (approx. 95 slices) compared to MRI (7 slices). This does not take away the advantage of the use of MRI in longitudinal studies when ex-vivo measurements are not possible. Also, MEMRI at higher concentrations has recently been shown to provide images of higher resolution that are comparable to histology (Shan et al., 2012). These issues concerning MRI and Mn concentrations will further be discussed in chapter 4.

3.5.2 Volumetric Analysis

There are no studies conducted on the effects of prenatal stress across 3 generations to compare to the current study. Therefore the comparisons were among F3 TPS stress to stress across one generation or chronic stress in general. There are only a few studies that analyzed volumetric measurements in prenatally stressed animals. A 3% reduction in hippocampal brain volume of stressed rats was found. Only one other study of volumetric measurements was performed in rodents. After subjecting pregnant dams to restraint stress their study showed that hippocampal wet weights of 3-month-old offspring were reduced by 15.4% in PS males and by 8.2% in PS females (Szuran et al., 1994). Also, studies have been performed in non-human primates. One study investigated hippocampal volume in rhesus monkeys and found a 10-12% reduction in the hippocampus (Coe et al., 2003) using *ex vivo* measurements, whereas another group found a 30% reduction (Uno et al., 1994). These reductions in hippocampal volumes are much greater than the reduction found in this study. The effects may be more similar to rats exposed to chronic stress as the present results are more comparable to a study which found a 3% reduction in rats exposed to chronic stress (Lee et al., 2009). One explanation is the type of stressor used. All of the studies above differ in the timing of exposure to the stressor and type of stressor. These parameters have different effects on the HPA axis response in pregnant dams and may determine the effects of PS on brain development.

The present approach cannot directly address the underlying cellular mechanisms by which stress reduces the size of the hippocampus. The major theory in the field states that stress-related hypercortisolemia causes hippocampal atrophy (McEwen, 2000). The present findings are consistent with earlier reports of apoptosis, dendritic atrophy and a

decrease of neurogenesis associated with PS (Zhu et al., 2004, Lemaire et al., 2000, Gould et al., 1997). The present results are also consistent with findings that epigenetic imprints of environmental stress may persist through multiple generations (Zucchi et al., 2012).

Since the choice of brain regions studied is driven by previous anatomical, behavioral and cognitive findings on the effects of PS in the offspring, there might possibly exist other regions that are equally affected by PS or TPS (Charil et al., 2010). For this reason, a whole brain volumetric measurement was taken as well. A 7% reduction in whole brain volume was found. The percent difference of hippocampus to whole brain volumes did not change in TPS rats compared to control rats. This could indicate that the hippocampal volume changed as a function of whole brain volume. Many of the studies above did not include whole brain volume and relative differences. It is, therefore, impossible to compare the present hippocampal results with these studies. There is some research which suggests that stress could cause a reduction in whole brain volume, and not just the major areas of interest; hippocampus, amygdala and prefrontal cortex. One study found that PS reduced the number of immature microglia (Gomez-Gonzalez et al., 2010). During early development of the central nervous system, microglial cells exert multiple protective and organizational functions that are necessary for proper neural development (Kaur et al., 2007). The mechanisms underlying these volume reductions are largely unclear.

3.6 Conclusions

Taken together, this study showed that the brain volume of animals that are multigenerationally stressed was negatively affected. The results validate the hypothesis that the parental stress effect is transferred to the filial generation and their progeny. A 3% reduction in hippocampal volume and a 7% reduction in whole brain volume compared to controls were found. MRI findings differed from histological measurements in number but not direction of change. To my knowledge, this is the first study which has shown volume reduction in rat brains of generationally stressed rats with the use of MRI. Also shown was an application of MEMRI and also included were some suggestions to improve the application. When Mn is released slowly with the use of an osmotic pump, there is a visible reduction in T1-relaxation in the hippocampus. A general discussion on technical difficulties and considerations from this study will be provided in Chapter 4.

Future Studies

For future studies, it would be very interesting to see if a higher concentration of Mn could show differences in brain activity between TPS rats or stressed rats in general compared to controls. Also, there have been many reports of changes in stress response between male and females. It would be interesting to investigate these changes using MEMRI. Another interesting study would be to compare brain volumes from F1-F3 generations. Additionally, studies on methods of reversing neurobiological effects of stress would also be interesting and the use of MEMRI would be a great addition to these longitudinal studies. As you can see, there are many promising opportunities for further research in this area.

3.7 References

Bryan RM (1990) Cerebral Blood-Flow and Energy-Metabolism during Stress. American Journal of Physiology 259:H269-H280.

Charil A, Laplante DP, Vaillancourt C, King S (2010) Prenatal stress and brain development. Brain research reviews 65:56-79.

Chaudhri OB, Parkinson JR, Kuo YT, Druce MR, Herlihy AH, Bell JD, Dhillo WS, Stanley SA, Ghatei MA, Bloom SR (2006) Differential hypothalamic neuronal activation following peripheral injection of GLP-1 and oxyntomodulin in mice detected by manganese-enhanced magnetic resonance imaging. Biochemical and biophysical research communications 350:298-306.

Coe CL, Kramer M, Czéh B, Gould E, Reeves AJ, Kirschbaum C, Fuchs E (2003) Prenatal stress diminishes neurogenesis in the dentate gyrus of juvenile Rhesus monkeys. Biological Psychiatry 54:1025-1034.

Cortez CM, Cruz FAD, Silva D (2008) Psycological and Physiological Responses to Stress: A Review Based on Results from PET and MRI Studies. Brazilian Archives of Biology and Technology 51:7-12.

Crews D, Gillette R, Scarpino SV, Manikkam M, Savenkova MI, Skinner MK (2012) Epigenetic transgenerational inheritance of altered stress responses. Proceedings of the National Academy of Sciences of the United States of America 109:9143-9148.

Eker C, Gonul AS (2010) Volumetric MRI studies of the hippocampus in major depressive disorder: Meanings of inconsistency and directions for future research. World Journal of Biological Psychiatry 11:19-35.

Eriksson H, Lenngren S, Heilbronn E (1987) Effect of long-term administration of manganese on biogenic amine levels in discrete striatal regions of rat brain. Archives of toxicology 59:426-431.

Eriksson R, Johansson L, Bjerner T, Ahlstrom H (2005) Dobutamine-induced stress affects intracellular uptake of manganese: A quantitative magnetic resonance imaging study in pigs. Journal of Magnetic Resonance Imaging 21:360-364.

Fride E, Dan Y, Feldon J, Halevy G, Weinstock M (1986) Effects of prenatal stress on vulnerability to stress in prepubertal and adult rats. Physiology & behavior 37:681-687.

Frodl T, Reinhold E, Koutsouleris N, Reiser M, Meisenzahl EM (2010) Interaction of childhood stress with hippocampus and prefrontal cortex volume reduction in major depression. Journal of Psychiatric Research 44:799-807.

Golub Y, Kaltwasser SF, Mauch CP, Herrmann L, Schmidt U, Holsboer F, Czisch M, Wotjak CT (2011) Reduced hippocampus volume in the mouse model of Posttraumatic Stress Disorder. Journal of Psychiatric Research 45:650-659.

Gomez-Gonzalez B, Escobar A (2010) Prenatal stress alters microglial development and distribution in postnatal rat brain. Acta neuropathologica 119:303-315.

Gould E, McEwen BS, Tanapat P, Galea LAM, Fuchs E (1997) Neurogenesis in the dentate gyrus of the adult tree shrew is regulated by psychosocial stress and NMDA receptor activation. J Neurosci 17:2492-2498.

Hankir MK, Parkinson JR, Minnion JS, Addison ML, Bloom SR, Bell JD (2011) Peptide YY 3-36 and pancreatic polypeptide differentially regulate hypothalamic neuronal

activity in mice in vivo as measured by manganese-enhanced magnetic resonance imaging. Journal of neuroendocrinology 23:371-380.

Henry C, Kabbaj M, Simon H, Le Moal M, Maccari S (1994) Prenatal stress increases the hypothalamo-pituitary-adrenal axis response in young and adult rats. Journal of neuroendocrinology 6:341-345.

Hui JJ, Zhang ZJ, Liu SS, Xi GJ, Zhang XR, Teng GJ, Chan KC, Wu EX, Nie BB, Shan BC, Li LJ, Reynolds GP (2011) Hippocampal neurochemistry is involved in the behavioural effects of neonatal maternal separation and their reversal by post-weaning environmental enrichment: A magnetic resonance study. Behavioural Brain Research 217:122-127.

Jackson SJ, Hussey R, Jansen MA, Merrifield GD, Marshall I, MacLullich A, Yau JL, Bast T (2011) Manganese-enhanced magnetic resonance imaging (MEMRI) of rat brain after systemic administration of MnCl(2): hippocampal signal enhancement without disruption of hippocampus-dependent behavior. Behav Brain Res 216:293-300.

Kalisch R, Schubert M, Jacob W, Kessler MS, Hemauer R, Wigger A, Landgraf R, Auer DP (2006) Anxiety and hippocampus volume in the rat. Neuropsychopharmacology : official publication of the American College of Neuropsychopharmacology 31:925-932.

Kaur C, Dheen ST, Ling EA (2007) From blood to brain: amoeboid microglial cell, a nascent macrophage and its functions in developing brain. Acta Pharmacol Sin 28:1087-1096.

Koolhaas JM, Bartolomucci A, Buwalda B, de Boer SF, Flugge G, Korte SM, Meerlo P, Murison R, Olivier B, Palanza P, Richter-Levin G, Sgoifo A, Steimer T, Stiedl O, van Dijk G, Wohr M, Fuchs E (2011) Stress revisited: a critical evaluation of the stress concept. Neuroscience and biobehavioral reviews 35:1291-1301.

Kuo YT, Herlihy AH, So PW, Bhakoo KK, Bell JD (2005) In vivo measurements of T1 relaxation times in mouse brain associated with different modes of systemic administration of manganese chloride. Journal of Magnetic Resonance Imaging 21:334-339.

Lee JH, Koretsky AP (2004) Manganese enhanced magnetic resonance imaging. Current Pharmaceutical Biotechnology 5:529-537.

Lee T, Jarome T, Li SJ, Kim JJ, Helmstetter FJ (2009) Chronic stress selectively reduces hippocampal volume in rats: a longitudinal magnetic resonance imaging study. Neuroreport 20:1554-1558.

Lemaire V, Koehl M, Le Moal M, Abrous DN (2000) Prenatal stress produces learning deficits associated with an inhibition of neurogenesis in the hippocampus. Proceedings of the National Academy of Sciences of the United States of America 97:11032-11037.

Lin YJ, Koretsky AP (1997) Manganese ion enhances T-1-weighted MRI during brain activation: An approach to direct imaging of brain function. Magnetic Resonance in Medicine 38:378-388.

Lucassen PJ, Bosch OJ, Jousma E, Kromer SA, Andrew R, Seckl JR, Neumann ID (2009) Prenatal stress reduces postnatal neurogenesis in rats selectively bred for high, but not low, anxiety: possible key role of placental 11beta-hydroxysteroid dehydrogenase type 2. The European journal of neuroscience 29:97-103.

Lui CC, Wang JY, Tain YL, Chen YC, Chang KA, Lai MC, Huang LT (2011) Prenatal stress in rat causes long-term spatial memory deficit and hippocampus MRI abnormality: Differential effects of postweaning enriched environment. Neurochemistry International 58:434-441.

McEwen BS (2000) The neurobiology of stress: from serendipity to clinical relevance. Brain research 886:172-189.

McEwen BS (2000) Protective and damaging effects of stress mediators: central role of the brain. Progress in brain research 122:25-34.

Migeon CJ, Prystowsky H, Grumbach MM, Byron MC (1956) Placental passage of 17-hydroxycorticosteroids: comparison of the levels in maternal and fetal plasma and effect of ACTH and hydrocortisone administration. The Journal of clinical investigation 35:488-493.

Morley-Fletcher S, Darnaudery M, Koehl M, Casolini P, Van Reeth O, Maccari S (2003) Prenatal stress in rats predicts immobility behavior in the forced swim test. Effects of a chronic treatment with tianeptine. Brain research 989:246-251.

Palacios RDY, Campo A, Henningsen K, Verhoye M, Poot D, Dijkstra J, Van Audekerke J, Benveniste H, Sijbers J, Wiborg O, Van der Linden A (2011) Magnetic Resonance Imaging and Spectroscopy Reveal Differential Hippocampal Changes in Anhedonic and Resilient Subtypes of the Chronic Mild Stress Rat Model. Biological Psychiatry 70:449-457.

Parkinson JR, Chaudhri OB, Kuo YT, Field BC, Herlihy AH, Dhillo WS, Ghatei MA, Bloom SR, Bell JD (2009) Differential patterns of neuronal activation in the brainstem and hypothalamus following peripheral injection of GLP-1, oxyntomodulin and lithium chloride in mice detected by manganese-enhanced magnetic resonance imaging (MEMRI). Neuroimage 44:1022-1031.

Porsolt R, Jalfre M (1978) Swimming Rats and Human Depression - Reply. Nature 274:512-513.

Ruiz RJ, Avant KC (2005) Effects of maternal prenatal stress on infant outcomes: a synthesis of the literature. ANS Advances in nursing science 28:345-355.

Shan D, Shaorui L, Yang L and Lei H (2012) Towards building a high resolution atlas of Mn2+ deposition in rat brain. Conference Proceedings, ISMRM Melbourne Australia

Szuran T, Zimmermann E, Welzl H (1994) Water Maze Performance and Hippocampal Weight of Prenatally Stressed Rats. Behavioural Brain Research 65:153-155.

Takahashi LK (1998) Prenatal stress: consequences of glucocorticoids on hippocampal development and function. International journal of developmental neuroscience : the official journal of the International Society for Developmental Neuroscience 16:199-207.

Takahashi LK, Turner JG, Kalin NH (1998) Prolonged stress-induced elevation in plasma corticosterone during pregnancy in the rat: implications for prenatal stress studies. Psychoneuroendocrinology 23:571-581.

Takahashi M, Odano I, Fujita S, Ohkubo M (1997) 125I-iomazenil binding shows stress- and/or diazepam-induced reductions in mouse brain: supporting data for 123I-iomazenil SPECT study of anxiety disorders. Annals of nuclear medicine 11:243-250.

Uno H, Eisele S, Sakai A, Shelton S, Baker E, Dejesus O, Holden J (1994) Neurotoxicity of Glucocorticoids in the primate. Hormones and Behavior 28:336-348.

Verstynen T, Tierney R, Urbanski T, Tang A (2001) Neonatal novelty exposure modulates hippocampal volumetric asymmetry in the rat. Neuroreport 12:3019-3022.

Williams MT, Davis HN, McCrea AE, Hennessy MB (1999) Stress during pregnancy alters the offspring hypothalamic, pituitary, adrenal, and testicular response to isolation on the day of weaning. Neurotoxicology and teratology 21:653-659.

Wolf OT, Dyakin V, Patel A, Vadasz C, de Leon MJ, McEwen BS, Bulloch K (2002) Volumetric structural magnetic resonance imaging (MRI) of the rat hippocampus following kainic acid (KA) treatment. Brain research 934:87-96.

Woods SM, Melville JL, Guo Y, Fan MY, Gavin A (2010) Psychosocial stress during pregnancy. American journal of obstetrics and gynecology 202:61 e61-67.

Yang J, Han H, Cao J, Li L, Xu L (2006) Prenatal stress modifies hippocampal synaptic plasticity and spatial learning in young rat offspring. Hippocampus 16:431-436.

Zach P, Mrzilkova J, Rezacova E, Stuchlik A, Vales K (2010) Delayed Effects of Elevated Corticosterone Level on Volume of Hippocampal Formation in Laboratory Rat. Physiol Res 59:12.

Zhu Z, Li X, Chen W, Zhao Y, Li H, Qing C, Jia N, Bai Z, Liu J (2004) Prenatal stress causes gender-dependent neuronal loss and oxidative stress in rat hippocampus. Journal of neuroscience research 78:837-844.

Zucchi FC, Yao Y, Metz GA (2012) The secret language of destiny: stress imprinting and transgenerational origins of disease. Frontiers in genetics 3:96.

CHAPTER 4

General Conclusions on the use of MEMRI in Neuroscience

4.1 Summary

The main objective of this research was to apply MEMRI to studies in Neuroscience by first establishing the limitations concerning the use of MEMRI in live rats. In Chapter 2, a MEMRI protocol in rats for direct infusion of Mn into the lateral ventricle using a cannula and an implanted osmotic pump system was introduced. The neurotoxicity of Mn using single pellet reaching was analyzed. Optimization of the Mn application procedure to reduce neurotoxic effects by comparing the effects of a low and a high dose. In Chapter 3, MEMRI was applied to a filial generation of stressed rats using subcutaneously implanted osmotic pumps for systemic Mn administration. In both chapters, images obtained using the MEMRI technique were compared to histology.

As described in the previous chapters, MEMRI has vast applications in Neuroscience. Its abilities to detect brain anatomy were displayed in Chapter 2 and Chapter 3. Chapter 2 utilized a method for the application of Mn to the lateral ventricle. It was shown that a low dose delivery using a 7-day osmotic pump shows Mn detectable changes in MRI without causing adverse toxic effects. To my knowledge, this was the first MEMRI experiment in which Mn was slowly infused into the lateral ventricles. Chapter 3 showed that the brain volume of transgenerationally stressed animals is negatively affected. Using MEMRI and histology, a 3% reduction in hippocampal volume and a 7% reduction in whole brain volume was found. MRI findings differed from histological measurements in number but not direction of change. To my

knowledge, this was the first study which has shown volume reduction in the brains of generationally stressed rats using MEMRI.

Because it is relatively noninvasive, MEMRI allows for repeated or longitudinal studies to follow the progression of disease or changes in anatomy. Results from Chapter 3 showed that MEMRI has abilities in increasing signal intensity to visualize cytoarchitecture. Histological methodologies are predominantly applied for the analysis of structural changes. However, these methods are limited by numerous factors including the examination of pre-selected brain regions, tissue alteration by the fixation method, depiction of neuroanatomical structures at one distinct time point per animal, and the sheer effort needed to examine all areas of the brain. MEMRI has abilities to not only detect brain anatomy but also track changes over time, which has caused MEMRI to become one of the leading techniques in MRI. MEMRI at higher Mn concentrations and at higher MR field has been shown to provide images of higher resolutions that are comparable to histology (Bridge et al., 2006, Shan et al., 2012).

MEMRI not only allows structural research but also identification of activation differences of certain brain areas. Numerous studies have shown that systemic administration of $MnCl_2$ leads to an activation-dependent accumulation of Mn. In Chapter 3, the visualization of changes in activation between the control rats compared to the TPS rats was attempted. Unfortunately, the concentration used in this study was not high enough to show significant changes. The limitations of the osmotic pump which led to this low concentration used will be discussed below.

The experiments provided some of the basic tools and validation procedures necessary for broader applications of MEMRI in studies with rats. Through these studies

the abilities/disabilities of MEMRI in terms of delivery method, toxicity and technical considerations were demonstrated.

4.2 Methods of MEMRI

4.2.1 Systemic versus Direct Administration of Manganese

Many studies have explored the route of Mn injections, toxicity of injection dose, sensitivity to anatomical structure analysis and changes in signal intensity according to the time-course after injection. However, there is no consistent method for the administration of Mn. When choosing a method of administration, most researchers will base their decision on the type of study that they wish to conduct and the ease and efficiency of the delivery method. In the present study, two different methods were applied (SQ osmotic pump and continuous delivery using focal cannula), both of which were used to show whole brain anatomy in areas where Mn would be transported.

In Chapter 2, it was shown that a low dose delivery of 0.85 mM Mn to the lateral ventricles, using a 7 day osmotic pump, induces detectable changes in MRI without causing adverse toxic effects. Work in Chapter 2 showed that a concentration of 100 mM Mn delivered over 28 days is too high for a direct cannulation while 0.85 mM delivered over 7 days is too low. There are only two other studies which have used focal injections into the CSF to show whole brain anatomy (Liu et al., 2004, Jeong et al., 2012). Jeong et al. (2012) used a 20 mM concentration into the region of the cisterna magna. Their results suggest that 20 mM of $MnCl_2$ in a volume of 50 µl is a physiologically stable dose for ICV administration in the rat and provides an optimal image for structural analysis of a

rat brain 24 h after administration. However, in this study, it was not determined if behavior was affected. This will be vital for future studies.

In Chapter 3, Mn was released slowly with the use of a systemically implanted osmotic pump. Using a dose of 7.14 mg/kg (based on a rat weight of 350 g) there was a visible reduction in T1-relaxation in the hippocampus. The concentration used was the lowest systemic concentration applied in any MEMRI study (Lee et al., 2005). Most systemic studies use doses of 9-175 mg/kg. Compared to other studies, it was shown that a dose of 7.14 mg/kg did not produce sufficiently large changes in all brain areas. With this low concentration, all neurotoxic effects were avoided. Although from Chapter 2, it is clear that there are still toxicity issues to consider.

4.2.2 Toxicity

Some issues of toxicity from both the systemic and direct applications were experienced. Work in Chapter 2 revealed that a concentration of 100 mM Mn caused a lesion in the rat's brain. Surprisingly, there were no adverse effects on behavior that could be detected using the single pellet reaching task. However, the local toxicity of the injections may still need to be considered, depending on the application. A recent study tracing sensorimotor connections in the rat brain reported that acute injections of 100 mM $MnCl_2$ solutions in brain parenchyma cause glial reaction for Mn loads above 8 nmol and neuronal death for loads at or above 16 nmol (Canals et al., 2008).

Histological results from work in Chapter 3 showed no indication of neural toxicity. However, it was observed that the rats lost, on average, 8 grams of body weight with the highest weight loss being 20 grams. This could indicate that the systemic method

of Mn infusion may be more stressful on the rats compared to the direct infusion. Systemic administration may prove to be more toxic because of the number of organs and systems, which the solution surpasses in order to reach its destination. This has been shown in previous studies using systemic applications (Eschenko et al., 2010, Jackson et al., 2011). The direct injection using an osmotic pump showed no significant effect on the rat's body weight during the course of the study, including during the single pellet reaching task (Figure 2.9). Although the methods used were targeting different locations, both experiments used a slow release technique via an osmotic pump.

4.2.3 Advantages and Disadvantages of the Use of Osmotic Pumps

One can now also consider, as it is becoming more popular, a slow release technique of administering Mn through the use of an osmotic pump. Both experiments in Chapter 2 and Chapter 3 made use of the osmotic pump to deliver Mn. As with all methods, there are many benefits and downfalls to this technique. Osmotic pumps come in a variety of sizes with different volumes, rates and durations for the administration of Mn solution. This is both a benefit and a deterrent as it limits the range of concentrations and volumes. It also allows for the tracking of enhancement due to changes in Mn concentration over time. Furthermore it decreases the susceptibility to toxicity issues which could arise from using bolus injections.

In Chapter 2, it was shown that a concentration of 0.85 mM can be delivered safely to the rat brain using an osmotic pump. In a neuronal tract tracing study, it was demonstrated that Mn doses that resulted in dramatic cortical lesions when injected acutely into the brain parenchyma, can be safely applied to the brain when delivered from

low concentrated solutions with constant and extremely slow infusion rates. Suggesting that under such conditions Mn^{2+} is continuously transported away from the infusion site by neurons and detoxified glial cells, both factors contribute to prevent the tissue concentration to reach the toxic threshold (Canals et al., 2008). Canals et al. (2008) also found that the pump delivery method did not produce any adverse effects compared to the acute method.

In Chapter 3, it was shown that a concentration of 100 mM can be applied systemically with the use of an osmotic pump. However, because of the set volume and duration of the osmotic pumps, it is difficult to increase the concentration without compromising osmolarity. As shown in Chapter 3, the highest dose that would match osmolarity in the 200 µl pumps was around 7.14mg/kg. From the current literature, it is understood that in order to decrease toxicity, solutions should be equal to the osmolarity of the body (Eschenko et al., 2010). Therefore, a concentration of 100 mM in a 200 µL solution was used, which matched this osmolarity of 300 mOsm. Conversely, concentrations higher than 100 mM have been used in other studies. Recently, one study showed that osmotic pumps are suitable for delivering up to 30 mg/kg Mn within 24 hours in MEMRI studies using rodent models that address anatomical imaging, tract tracing and other neurological diseases (Sepulveda et al., 2012). This group used a larger osmotic pump with a volume of 2 ml. Another study achieved a significantly higher dose of Mn (180 mg/kg) than that employed in previous studies without any observable toxic effects on animal physiology or behavior (Mok et al., 2012). The pump volume used in this study was not stated; therefore it is unclear whether or not osmolarity was matched.

Although the pumps may compromise osmolarity, they are still very efficient at reducing toxic effects.

Eschenko et al. (2010) showed the importance of osmotic pumps to reduce toxic effects of Mn. Multiple injections conducted intraperitoneally in awake animals or intravenously in anesthetized animals was shown to be too intrusive for some behavioral studies (Eschenko et al., 2010). These authors then used IP osmotic pumps to deliver a total of 80 mg/kg of $MnCl_2$ over 7 days and found no decreases in motor performance. In contrast, an equivalent single bolus dose administered systemically was found to reduce wheel running, as well as food intake and body weight (Eschenko et al., 2010). This study showed the importance of the use of an osmotic pump to achieve continuous slow, systemic release of Mn in rats. The method of Mn infusion via osmotic pump implantation is thus less disruptive to the animal's mobility and could be very beneficial in studies of animal behavior.

Taken together, results from both studies indicate that a low concentration slowly infused into the lateral ventricles is suitable for a study of behavior and structure. We showed that for focal infusions concentrations of 0.85 mM Mn can be safely used. From the issues of toxicity, it was shown that systemic administration may cause more stress on the animal as the rats lost weight, whereas those who had focal infusion maintained their weight. There are also methods which can enable one the use of lower concentrations but achieve higher resolutions. These are technical issues which are discussed below.

4.3 Technical Considerations

In spite of the vast results, there were some technical difficulties that should be noted. Chapter 2 indicated that images obtained on some days had artifacts and were not useable. Chapter 3 discussed issues arising from the resolution obtained in the MRI images. First, it was difficult to determine the hippocampal boundaries on the images making it difficult to determine accurate hippocampal volume. This was due to a low contrast-to-noise ratio making it difficult to detect boundaries in regions with similar SNR. Second, the SNR obtained with the control images (taken a month after TPS rats were imaged) was of better quality. The variability in image quality was most likely due to an internal or external variable noise source beyond my control. Issues with the hardware and coil were faced during both studies presented here.

One issue concerns the use of a surface coil for signal detection. The advantage of this small surface coil was the high sensitivity close to the coil and the small area from where noise is received. Both of these factors contribute to good SNR. However, the sensitivity is highly inhomogeneous and results in a decreasing signal as a function of distance from the coil (Chuang and Koretsky, 2006). This leads to signal gradients in the image which degrades contrast to noise with depth and may affect volumetric measurements. Signal intensity was also sensitive to changes in tuning and matching of the coil, inhomogeneities in the excitation field (B1), receiver gain, and receive coil sensitivity. Our system has a manual setup, and all parameters need to be carefully set.

The issues above could also be present because the data were acquired with an MRI scanner that is considered to be of relatively low magnetic field strength. Most studies in MEMRI use a scanner of higher field strength (>4.7 T used in this study).

Achieving a high-field MRI is driven by the benefits of possibly higher signal-to-noise ratio, contrast-to-noise ratios and resolution for selected applications. In most cases, these benefits will enable higher spatial and/or temporal resolution than formerly possible with MRI. This is another factor which should be considered when choosing the concentration of Mn which should be used. MRI magnets of higher field strength (7 T and higher), are able to detect changes in T1 relaxation better than those of lower field because the normal tissue T1 is prolonged and the SNR is also higher at greater magnetic field strengths. It is therefore important to consider the equipment used to best suit the methodology applied.

Sampling at higher resolutions could also improve visualization of fine structures, such as full hippocampi. However, sampling at higher resolution also requires prolonged scanning time and hence extended anesthesia of the animal. Thus, the advantages of high resolution and the disadvantage of prolonged anesthesia have to be counterbalanced and adjusted to experimental demands. Furthermore, sampling at higher resolution also decreases SNR. However, smaller and more focal surface coils help in reducing this penalty as it decreases noise that could be detected from other structures. Technical advances in the field of imaging sequences for small animal MRI over the last few decades, the combination of different acquisition techniques, such as T1 mapping, and the adjusted scanning parameters for MEMRI should lead to a considerable improvement of images obtained using MEMRI (Lee et al., 2005; Chuang and Koretsky, 2006).

4.4 Conclusions

MEMRI has proven to be an asset to many studies in Neuroscience. These include studies of cytoarchitecture (Aoki et al., 2004), tract tracing (Chuang et al., 2006) and brain mapping (Eschenko et al., 2010) to name a few. The experiments in this thesis established two methods of Mn delivery, systemic and focal infusion. Also, an application for the use of MEMRI for volumetric analysis was successfully demonstrated. From the studies conducted here, it is evident that MEMRI has many advantages. MEMRI enabled a relatively quick overview of the whole brain *in vivo* to identify regions of the brain. Most studies lack the great advantage of MEMRI to measure structural neuroanatomy *in vivo*. Most importantly, MEMRI allowed for longitudinal studies which could give more detailed insight into the effects of training and learning on neuroanatomy. Overall, MEMRI has proved to be an invaluable tool in the field of neuroscience.

4.5 Future Directions

Many directions for future studies were introduced in Chapters 2 and 3. In general, attempts should be made to increase the sensitivity of MEMRI by optimizing the MRI hardware, MRI sequences and data analysis to allow for using the lowest possible Mn concentration for a specific biological question. The goal of establishing the MEMRI method has been to enable longitudinal studies without disturbing regional functionality. This requires further detailed investigation of Mn toxicology in terms of behavior and neurophysiological consequences. Also, as with most animal research, finding applications to human studies should also be considered. Several human Mn-based

contrast agents have been developed. GE Healthcare developed Teslascan for liver imaging (which has been discontinued since) (Vitellas et al., 2001). Currently, Eagle Vision Pharmaceutical Corp. (Exton, PA, USA) is testing another Mn-based contrast agent called SeeMore for heart imaging (Storey et al., 2006). However, despite these advancements, it is unknown if MEMRI for brain imaging will ever be used in humans. For now, however, animal studies are vital to improve overall understanding of MEMRI and its applications in brain imaging.

4.6 References

Aoki I, Wu YJL, Silva AC, Lynch RM, Koretsky AP (2004) In vivo detection of neuroarchitecture in the rodent brain using manganese-enhanced MRI. Neuroimage 22:1046-1059.

Bridge H, Clare S (2006) High-resolution MRI: in vivo histology? Philosophical transactions of the Royal Society of London Series B, Biological sciences 361:137-146.

Canals S, Beyerlein M, Keller AL, Murayama Y, Logothetis NK (2008) Magnetic resonance imaging of cortical connectivity in vivo. Neuroimage 40:458-472.

Chuang KH, Koretsky A (2006) Improved neuronal tract tracing using manganese enhanced magnetic resonance imaging with fast T-1 mapping. Magnetic Resonance in Medicine 55:604-611.

Eschenko O, Canals S, Simanova I, Beyerlein M, Murayama Y, Logothetis NK (2010) Mapping of functional brain activity in freely behaving rats during voluntary running using manganese-enhanced MRI: Implication for longitudinal studies. Neuroimage 49:2544-2555.

Jeong KY, Lee C, Cho JH, Kang JH, Na HS (2012) New Method of Manganese-Enhanced Magnetic Resonance Imaging (MEMRI) for Rat Brain Research. Experimental animals / Japanese Association for Laboratory Animal Science 61:157-164.

Lee JH, Silva AC, Merkle H, Koretsky AP (2005) Manganese-enhanced magnetic resonance imaging of mouse brain after systemic administration of MnCl2: dose-dependent and temporal evolution of T1 contrast. Magnetic resonance in medicine : official journal of the Society of Magnetic Resonance in Medicine / Society of Magnetic Resonance in Medicine 53:640-648.

Liu CH, D'Arceuil HE, de Crespigny AJ (2004) Direct CSF injection of MnCl2 for dynamic manganese-enhanced MRI. Magnetic Resonance in Medicine 51:978-987.

Mok SI, Munasinghe JP, Young WS (2012) Infusion-based manganese-enhanced MRI: a new imaging technique to visualize the mouse brain. Brain structure & function 217:107-114.

Sepulveda MR, Dresselaers T, Vangheluwe P, Everaerts W, Himmelreich U, Mata AM, Wuytack F (2012) Evaluation of manganese uptake and toxicity in mouse brain during continuous MnCl(2) administration using osmotic pumps. Contrast media & molecular imaging 7:426-434.

Storey P, Chen Q, Li W, Seoane PR, Harnish PP, Fogelson L, Harris KR, Prasad PV (2006) Magnetic resonance imaging of myocardial infarction using a manganese-based contrast agent (EVP 1001-1): preliminary results in a dog model. J Magn Reson Imaging 23:228-234.

Vitellas KM, El-Dieb A, Vaswani K, Bennett WF, Fromkes J, Steinberg S, Bova JG (2001) Detection of bile duct leaks using MR cholangiography with mangfodipir trisodium (Teslascan). Journal of computer assisted tomography 25:102-105.

APPENDIX A: Single Pellet Reaching Task Rating Scale

1. Orient	-Head oriented to target	_____	_____	_____
	-sniffing	_____	_____	_____
2. Limb Lift	-body weight shift to back	_____	_____	_____
	-hindlimbs aligned with body	_____	_____	_____
	-limb moves forward	_____	_____	_____
	-digits on midline	_____	_____	_____
3. Digits Close	-palm supinated, semi-in	_____	_____	_____
	-digits semiflexed	_____	_____	_____
4. Aim	-elbows come in	_____	_____	_____
	-palm in midline	_____	_____	_____
5. Advance	-elbow in	_____	_____	_____
	-limb forward	_____	_____	_____
	-limb directed to target	_____	_____	_____
	-head and upper body raised	_____	_____	_____
	-body weight shift front	_____	_____	_____
	-body weight shift lateral	_____	_____	_____
6. Digits Open	-digits open	_____	_____	_____
	-discrete limb movement	_____	_____	_____
	-not fully protonated	_____	_____	_____
7. Pronation	-elbow out	_____	_____	_____
	-palm down in arpeggio	_____	_____	_____
8. Grasp	-arm still	_____	_____	_____
	-digits close	_____	_____	_____
	-hand lifts	_____	_____	_____
9. Supination I	-elbow in	_____	_____	_____
	-palm medially before leaving slot	_____	_____	_____
	-palm turned 90^{o}	_____	_____	_____
10. Sup. II	-head points down	_____	_____	_____
	-body horizontally	_____	_____	_____
	-palm straight up	_____	_____	_____
	-distal limb movement	_____	_____	_____
11. Release	-open digits	_____	_____	_____
	-puts food in mouth	_____	_____	_____
	-head and upper body lowered	_____	_____	_____
	-raises other paw	_____	_____	_____

APPENDIX B: Protocol for Cresyl Violet Histology

Cresyl Violet Histology

Sequence for dipping slides:

START

6 **Cresyl** **1min PRN** **(as needed)**	**5** **dH2O** **1min**	**4** **dH2O** **1min**	**3** **70% EtOH** **2min**	**2** **95% EtOH** **2min**	**1** **Abs EtOH** **2min**
7 **dH2O** **rinse**	**8** **70% EtOH** **2min**	**9** **95% EtOH** **2min**	**10** **Abs EtOH** **2min**	**11** **Diff.** **2 min PRN**	**12** **95% EtOH** **30 sec**
16 **Mount in** **HemoDe**	**Transfer to** **Fume Hood**	**Keep in** **HemoDe**	**15** **HemoDe** **5min**	**14** **HemoDe** **(solvent)** **5min**	**13** **Abs EtOH** **1min**

END